Analyses of visible images of the plasma periphery observed with tangentially viewing CCD cameras in the Large Helical Device

M. Shoji, T. Watanabe, S. Masuzaki, H. Yamada,
A. Komori and LHD Experimental Groups

National Institute for Fusion Science, Toki 509-5292, Japan

Contents

- Large Helical Device (LHD)
- Magnetic Field Line Structure in the Plasma Periphery
- Dependence of the Magnetic Field Line Structure on Magnetic Parameters (γ, R_{ax}, B_q)
- Tangentially Viewing CCD Cameras for monitoring plasmas
- Observed Images of Visible Emission with the Cameras
- Three-dimensional Plots of Magnetic Field Lines
- Toroidal/Poloidal Distribution of Strike Points
- Summary

Abstract

Complicated images of the visible emission profiles have been observed with tangentially viewing CCD cameras for monitoring LHD plasmas. These images strongly depend on magnetic parameters which specify the magnetic configuration in the plasma periphery (γ, R_{ax}, B_q).

We investigate these profiles from the viewpoint of the magnetic field line configurations in the plasma periphery by tracing magnetic field line with the three-dimensional model of the vacuum vessel and the helical coil cans including the geometrical data of the position and size of the divertor plates.

The analyses reveal that the complicated images of the visible emission can be explained by the three-dimensional configurations of the magnetic field in the plasma periphery, showing that plasma flow along the magnetic field lines is dominant in the LHD plasma periphery.

Basing on the above analyses, we calculate the toroidal and poloidal positions and distribution of strike points in various magnetic configurations, which proposes a safe operational range of magnetic configurations in order to minimize the direct heat load to the vacuum vessel (not high temperature materials).

Large Helical Device (LHD)

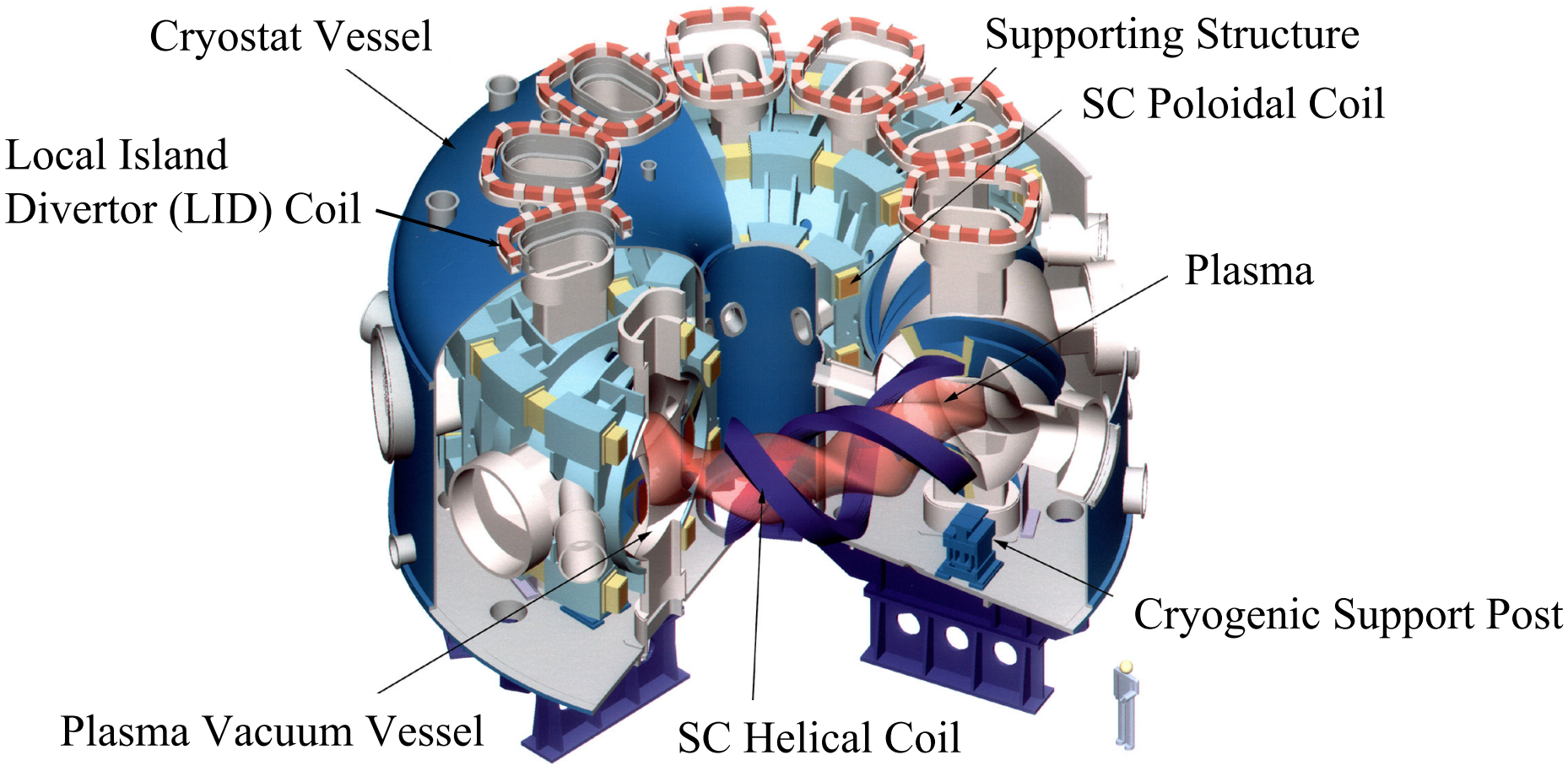

Toroidally twisted magnetic configurations are formed by the two twisted helical coils and circular poloidal coils. These super-conducting coils can effectively contribute to perform stable plasma discharge operation in LHD.

Magnetic Field Line Structure in LHD Plasmas

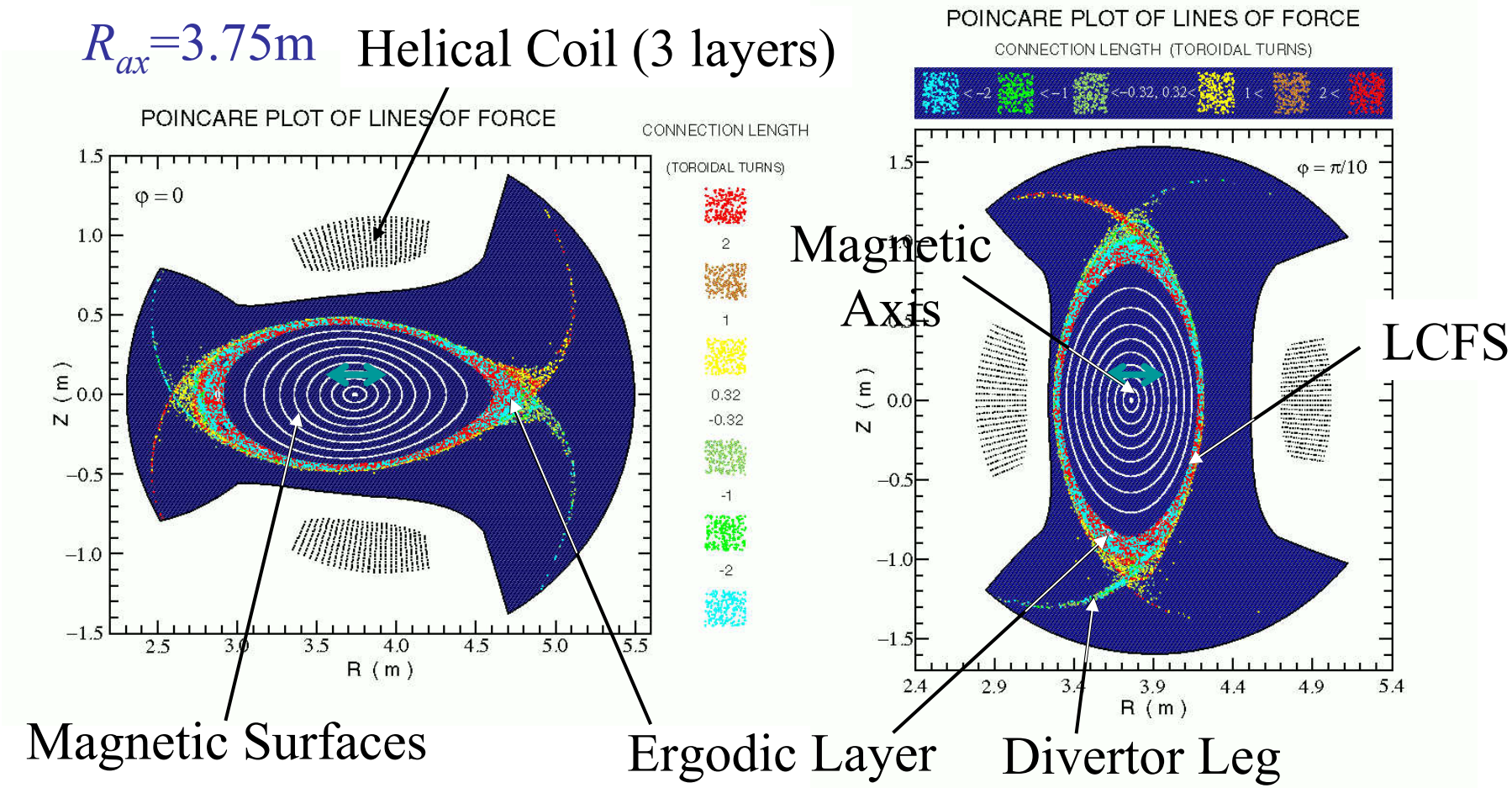

Ergodic layer with four divertor legs is formed around the last close flux surface (LCFS). The position of the magnetic axis (R_{ax}) can be flexibly changed by the poloidal and helical coils which also changes the magnetic configurations in the plasma periphery (ergodic layer) and the divertor legs.

Dependence of Magnetic Field Line Structure on γ

R_{ax}=3.60, B_q=100%

γ=1.13, 1.15, 1.18, 1.20, 1.22, 1.254, 1.265

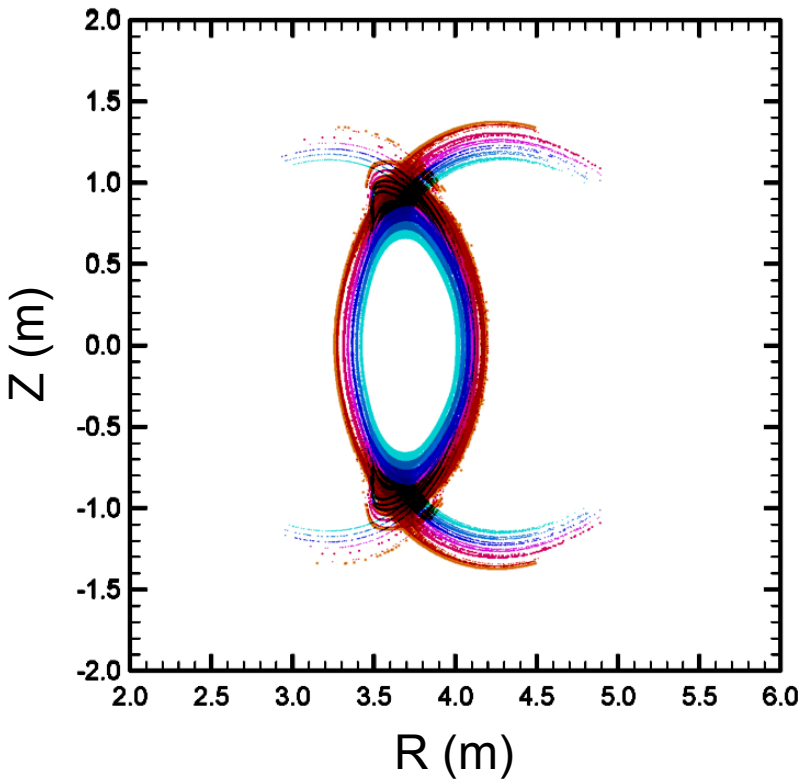

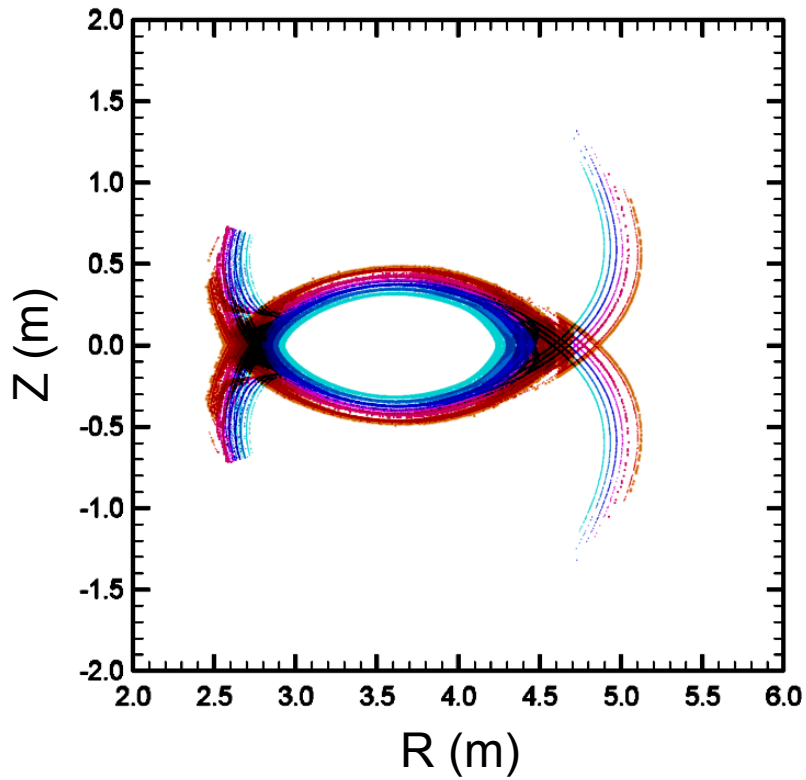

The size of the last closed flux surface (LCFS) increases in the coil pitch parameter (γ). The position of the separatrix (cross point of the divertor legs) is moved by the coil pitch parameter.

Dependence of Magnetic Field Line Structure on R_{ax}

γ=1.254, B_q=100%

R_{ax}=3.50, 3.55, 3.60, 3.65, 3.70, 3.75, 3.90, 4.05 m

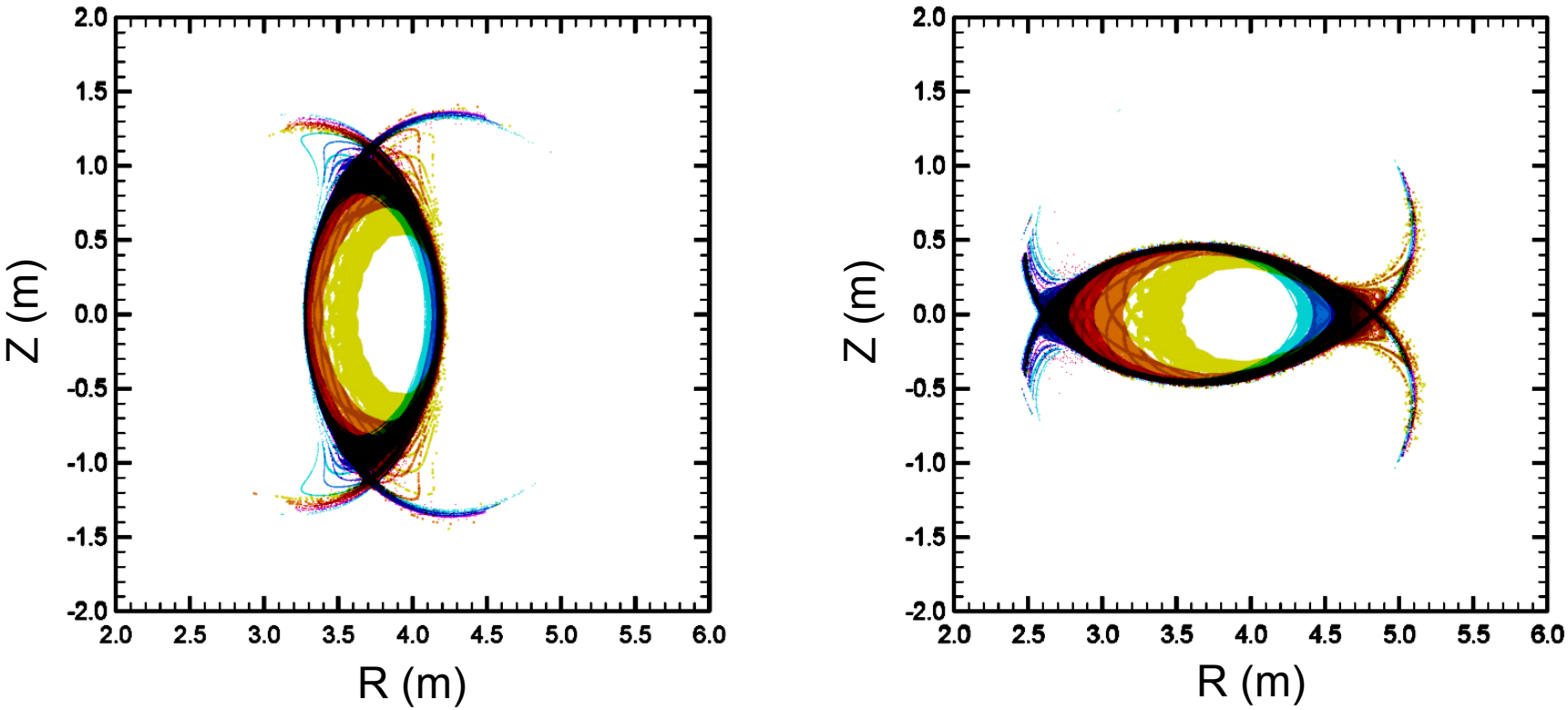

Magnetic configurations in the plasma periphery are changed with the radial position of the magnetic axis (R_{ax}). The position of the separatrix (cross point of the divertor legs) is not significantly moved by the magnetic axis.

Dependence of Magnetic Field Line Structure on B_q

R_{ax}=3.60, γ=1.254

B_q=-200, -150, -100, -50, 0, 72, 100, 150, 200 %

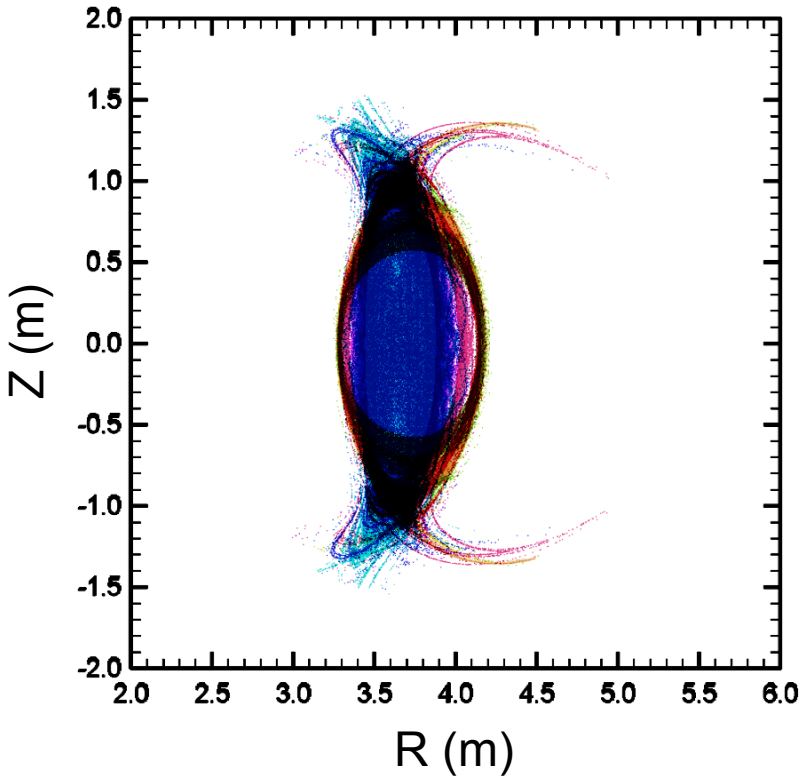

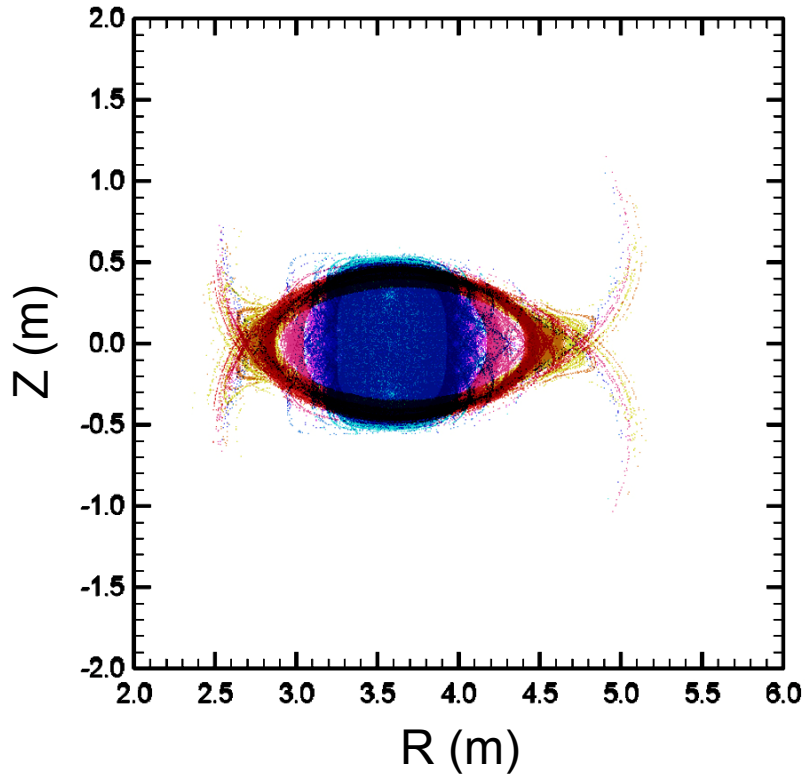

Magnetic configurations in the plasma periphery are changed with the quadrupole magnetic component (B_q). The position of the separatrix (cross point of the divertor legs) is not significantly moved by the component.

Position of Tangentially Viewing CCD Cameras

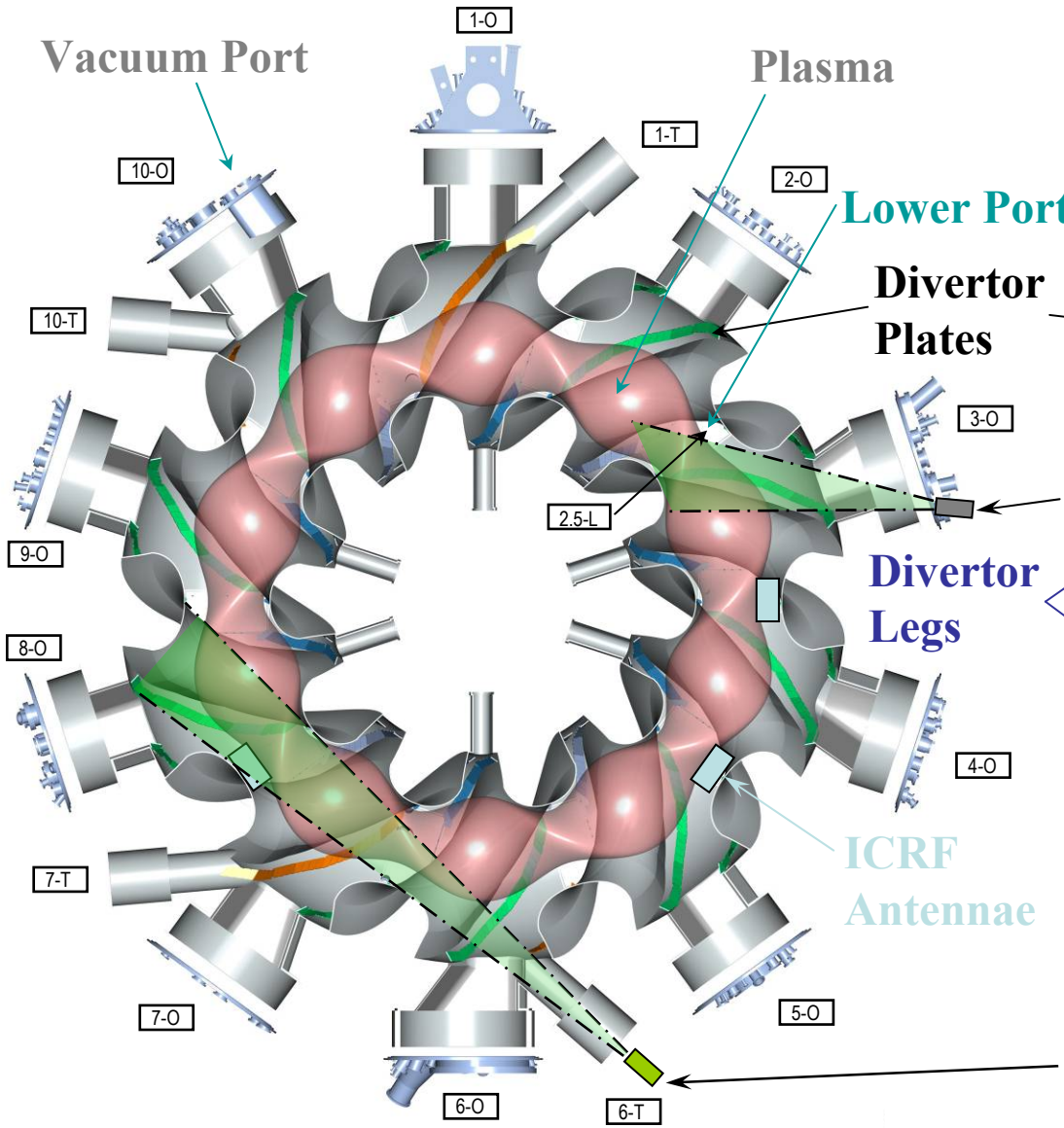

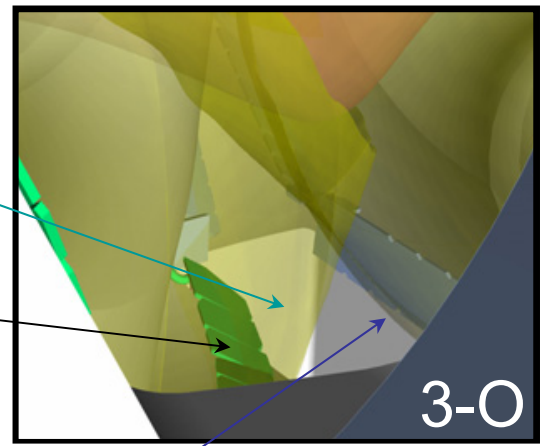

CCD camera for monitoring lower divertor plates

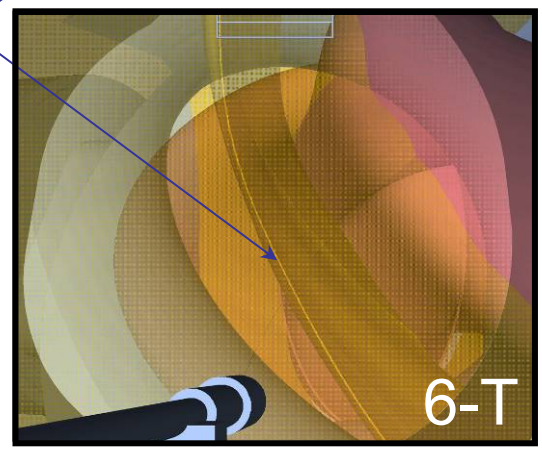

CCD camera for monitoring whole plasma tangentially

CCD cameras are installed for monitoring LHD plasmas and divertor plates.

Images of Visible Emission Observed with the Cameras

Dependence of γ, R_{ax}=3.60m, B_q=100%

γ=1.129 γ=1.15 γ=1.18

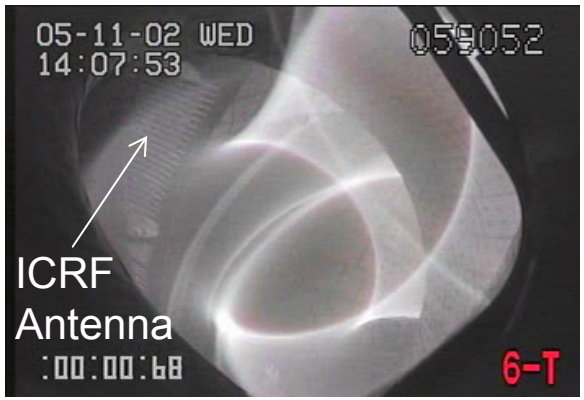

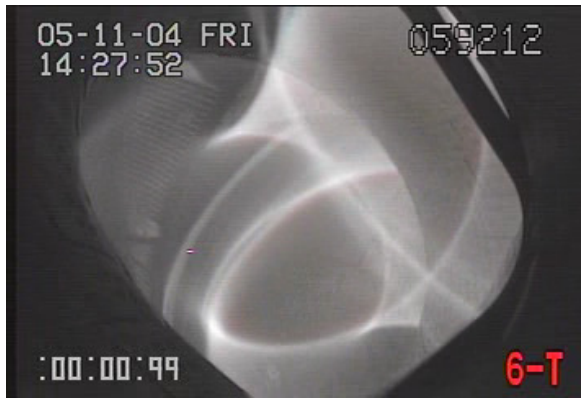

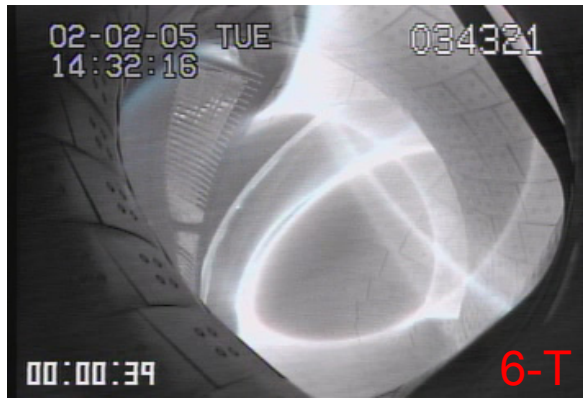

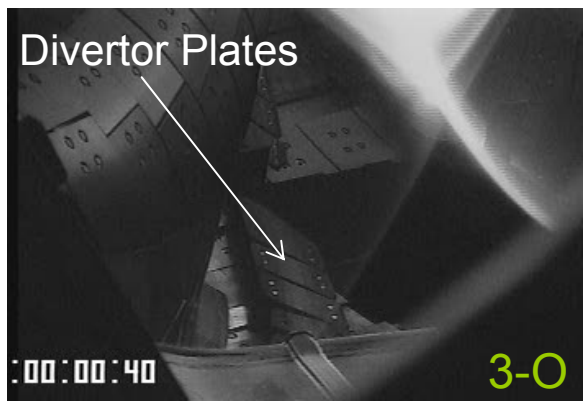

The area of the visible emission profile in the minor radius observed from a tangential port (6-T) increases in the coil pitch parameter (γ).

Three-dimensional Model of Magnetic Field Lines

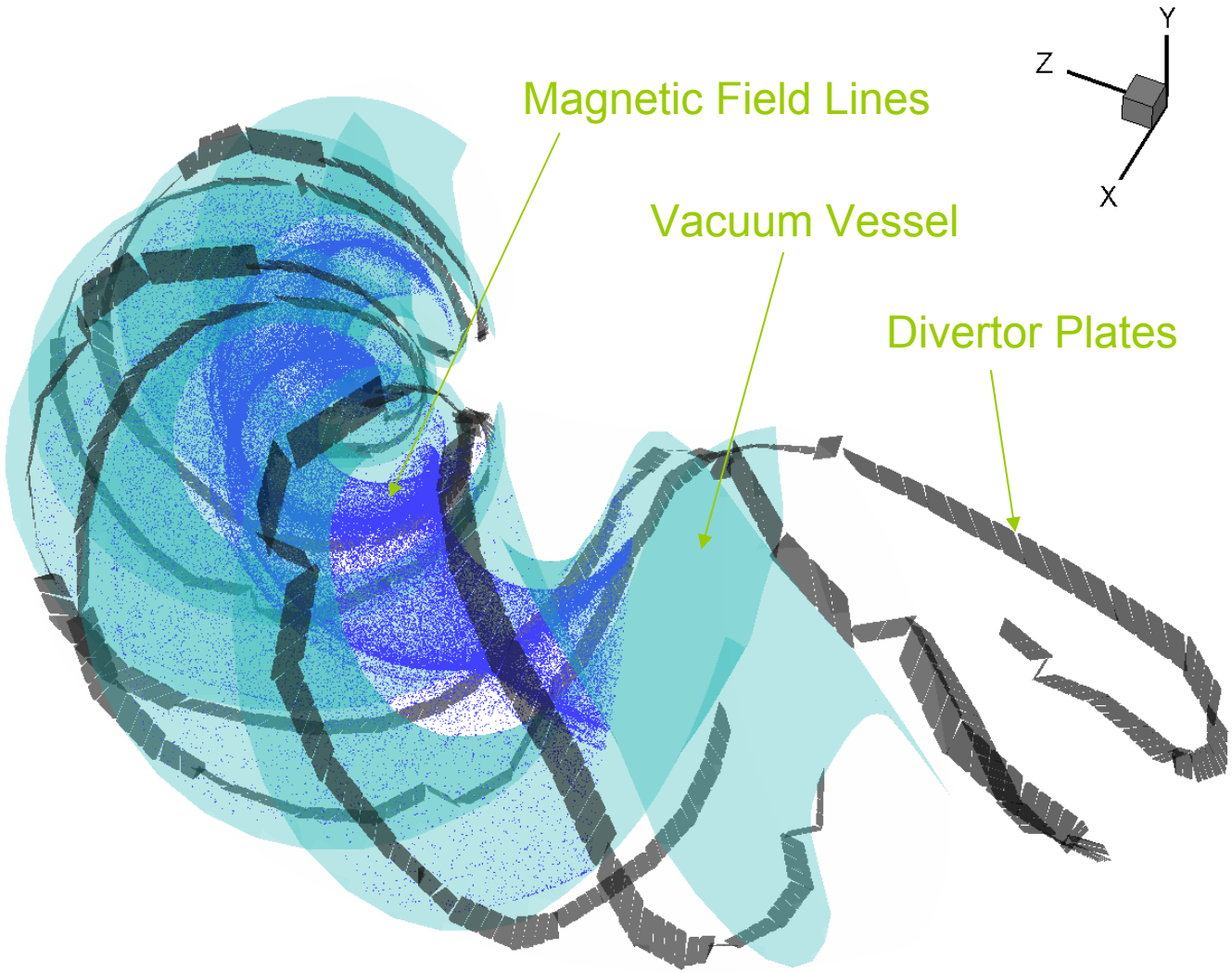

For analyses of the observed images, magnetic field lines are traced in a 3-D model including the geometry of the vacuum vessel and divertor plates.

Images of the 3-D Plots of the Magnetic Field Lines

γ=1.13

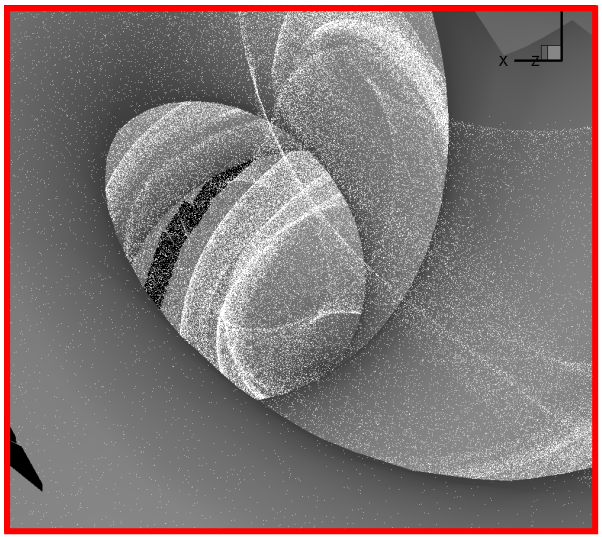

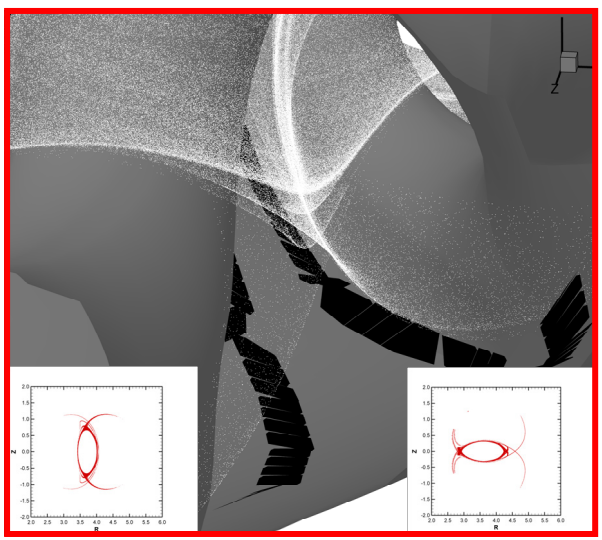

γ=1.15

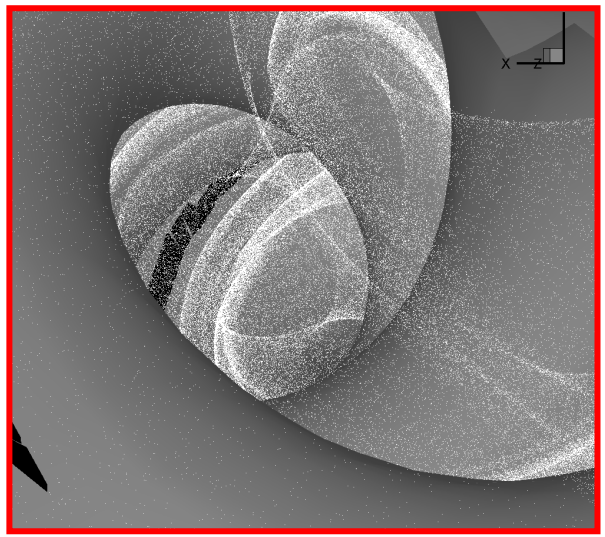

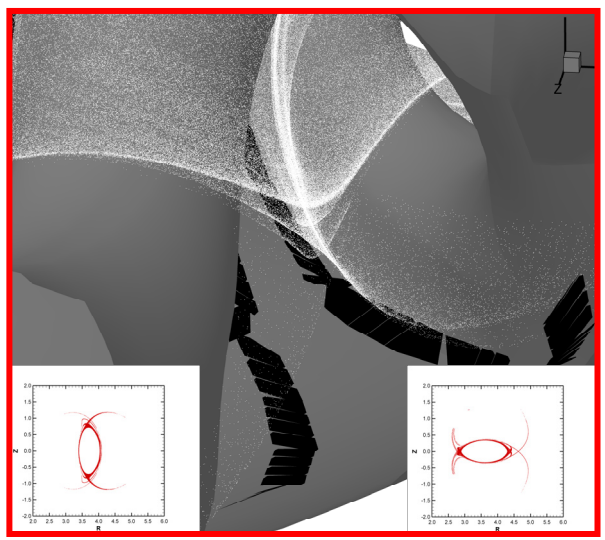

γ=1.18

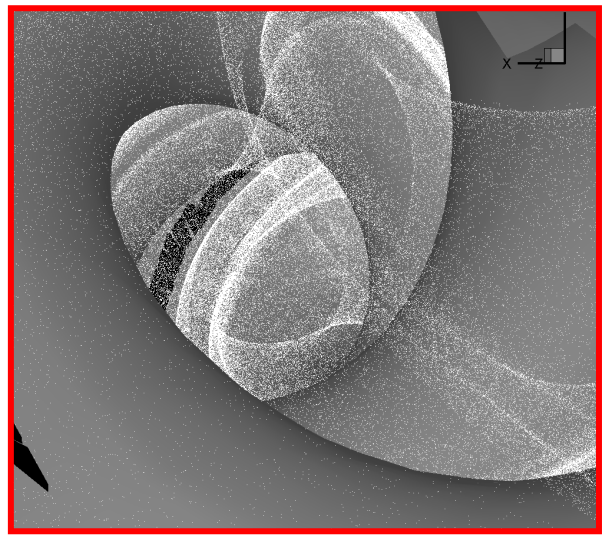

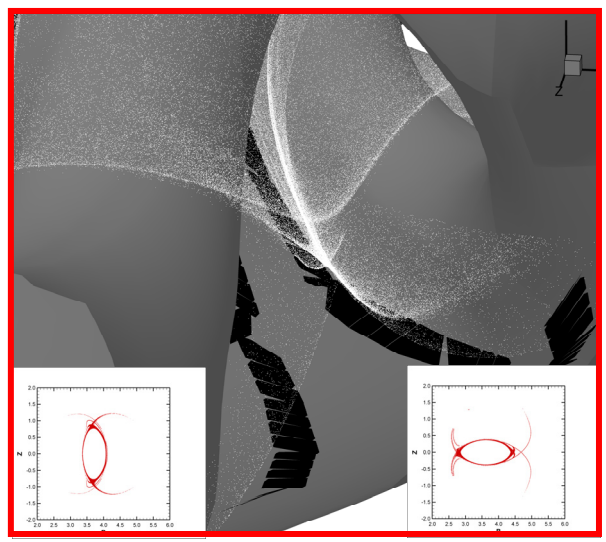

Toroidal and Poloidal Distribution of Strike Points

γ=1.13

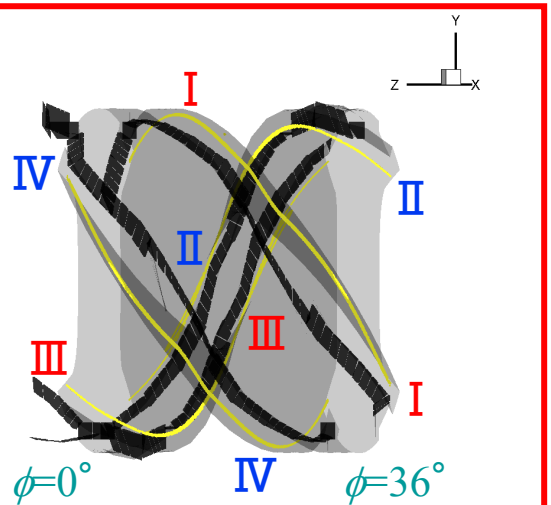

γ=1.15

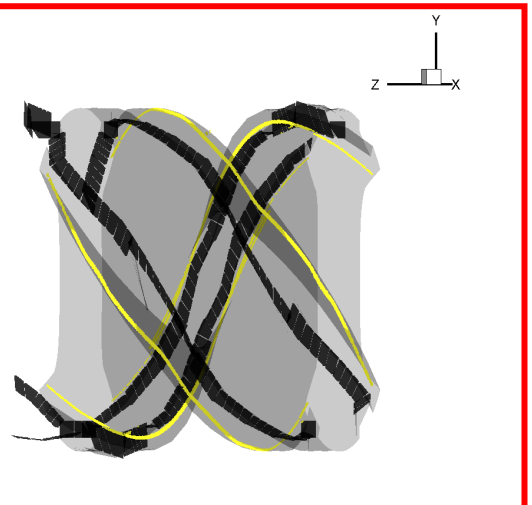

γ=1.18

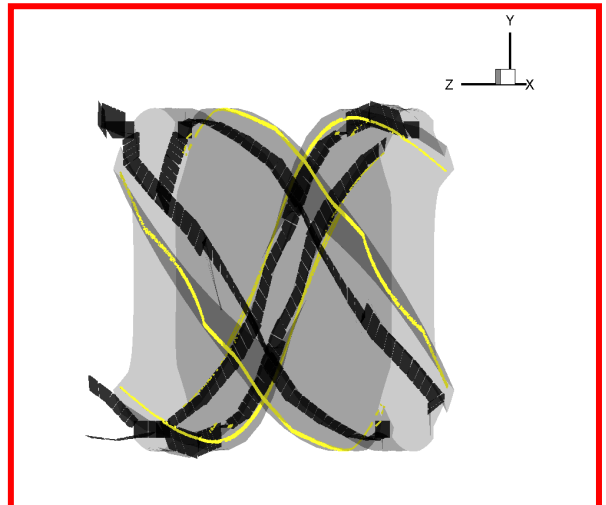

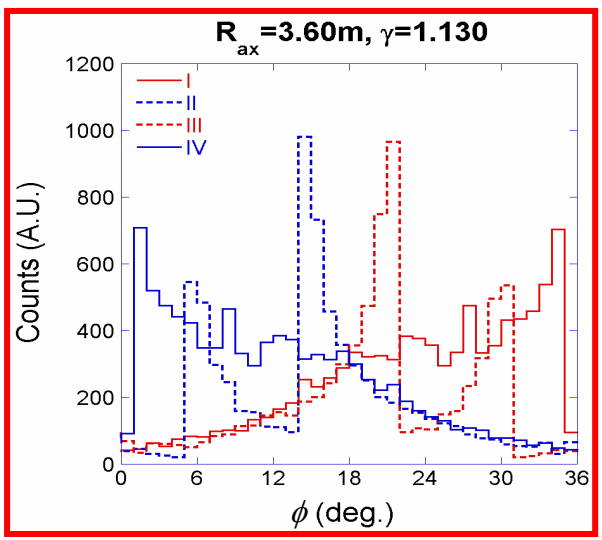

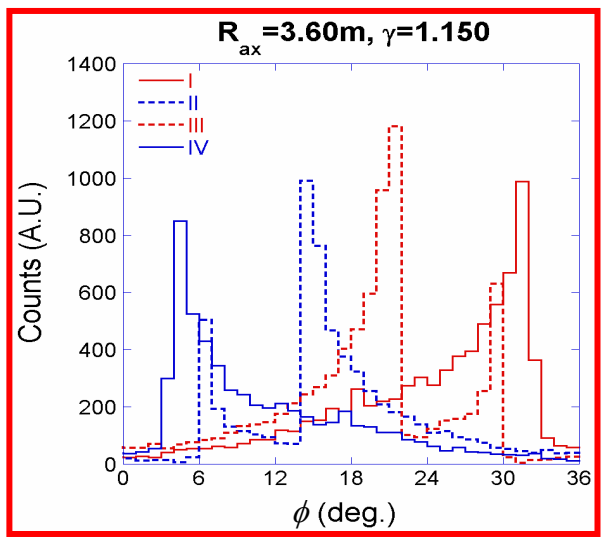

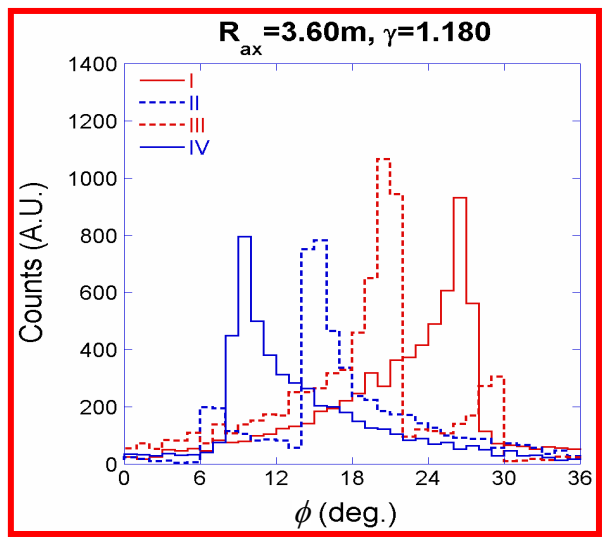

Images of Visible Emission Observed with the Cameras

Dependence of γ, R_{ax}=3.60m, B_q=100%

γ=1.2	γ=1.22	γ=1.254
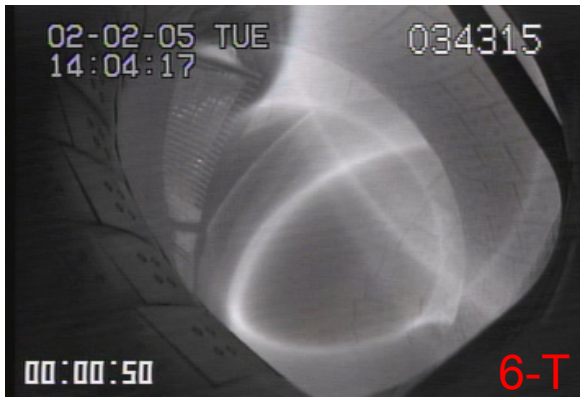	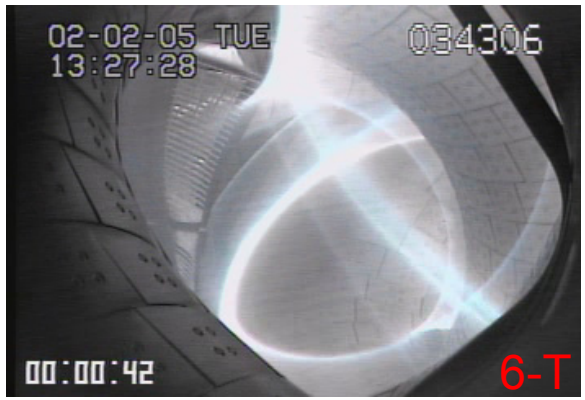	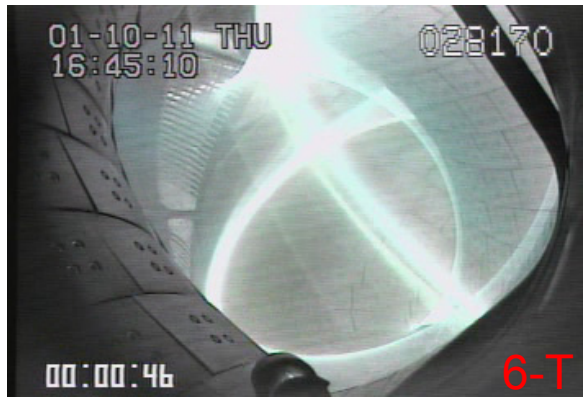
	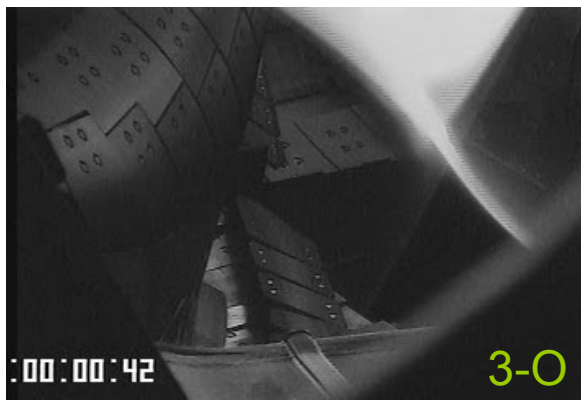	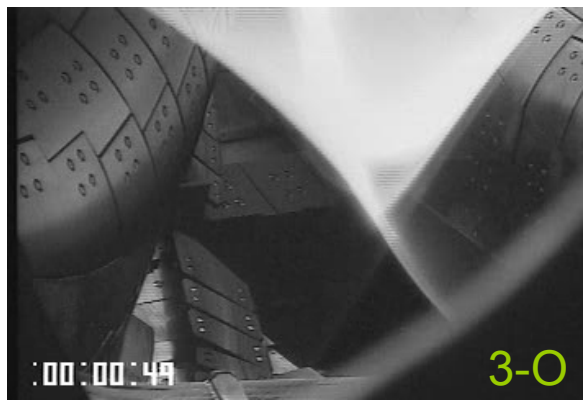

The area of the visible emission profile in the minor radius observed from a tangential port (6-T) increases in the coil pitch parameter (γ).

Images of the 3-D Plots of the Magnetic Field Lines

γ=1.20	γ=1.22	γ=1.254
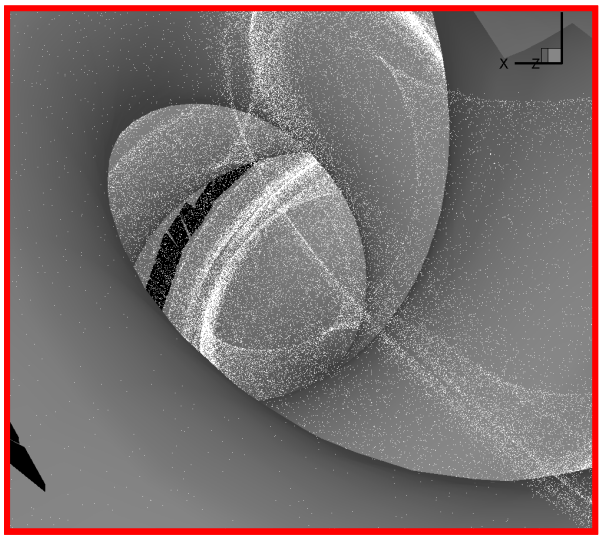	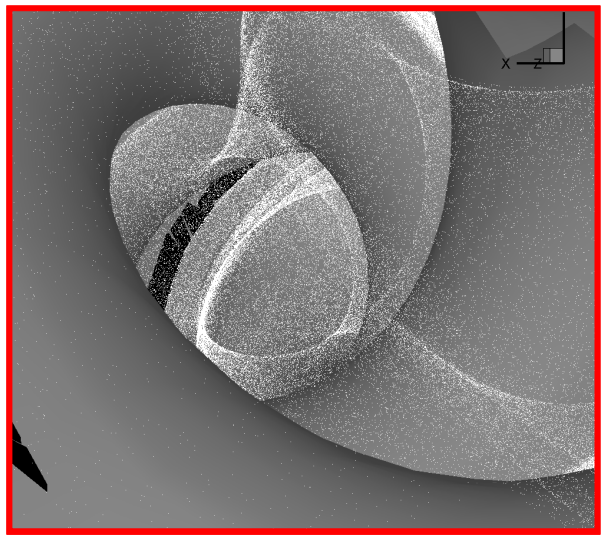	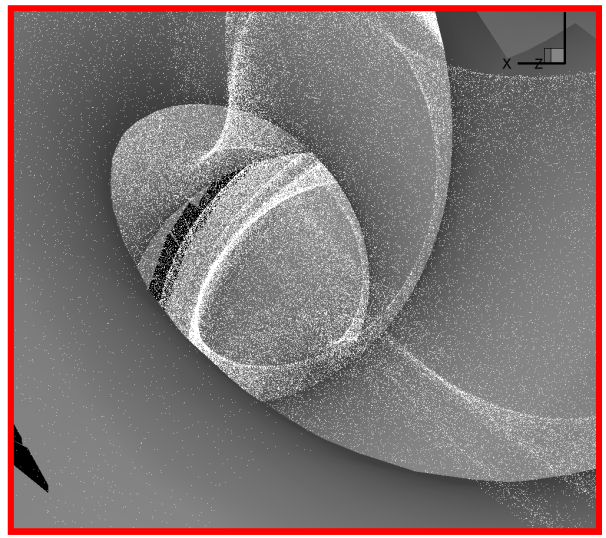
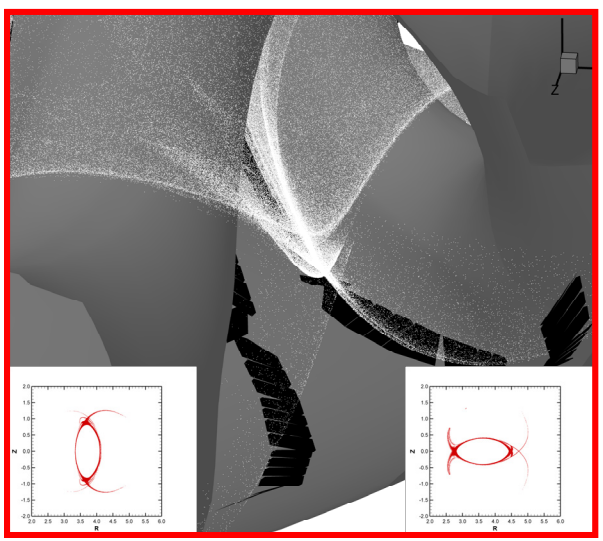	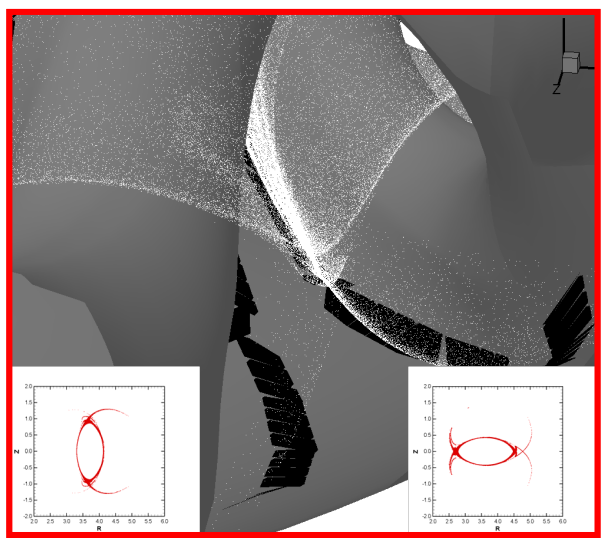	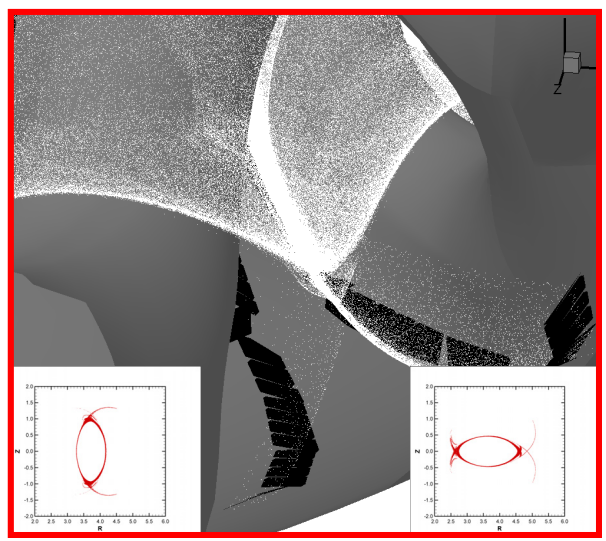

Toroidal and Poloidal Distribution of Strike Points

γ=1.20

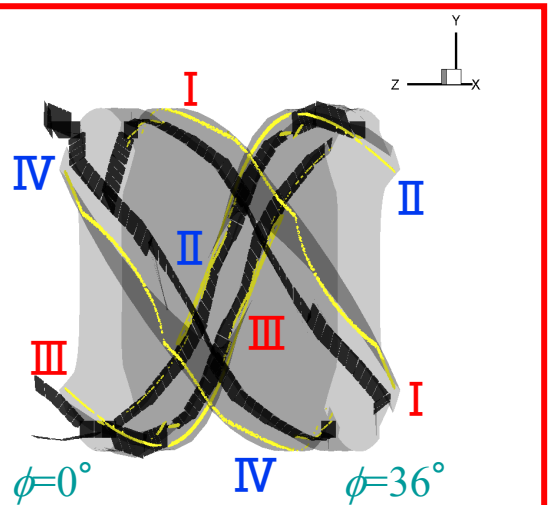

γ=1.22

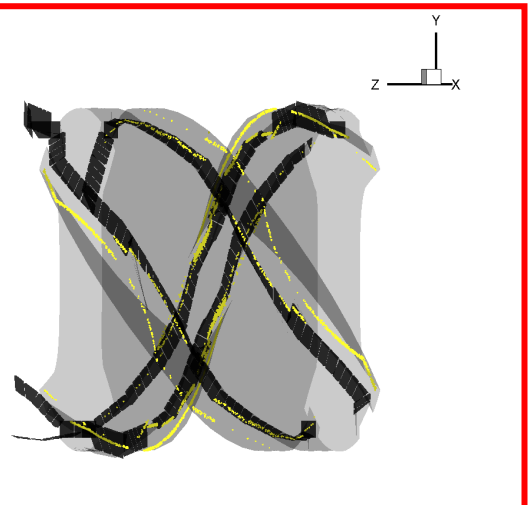

γ=1.254

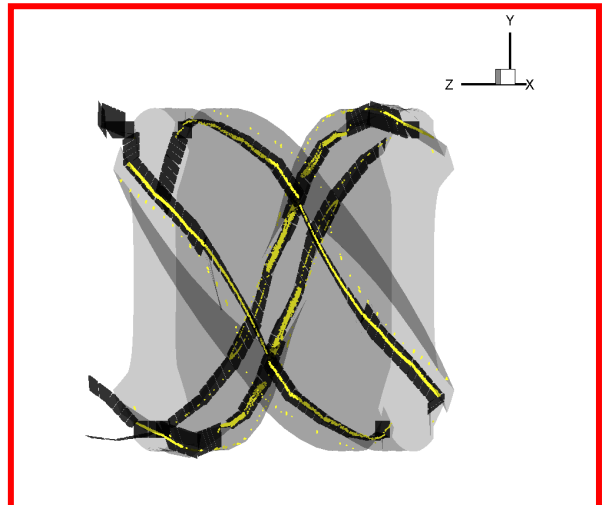

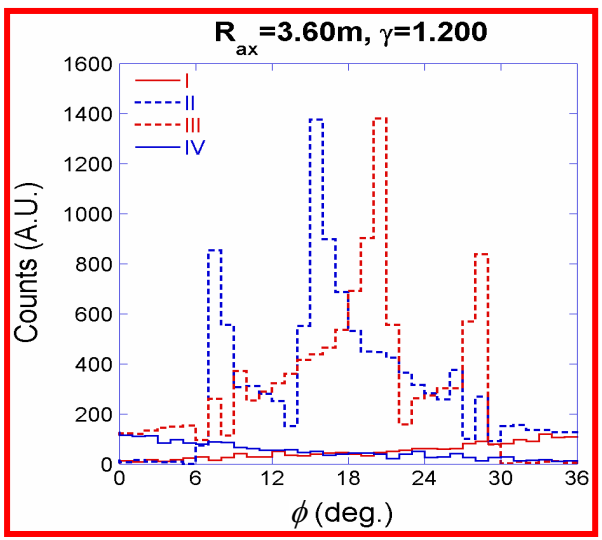

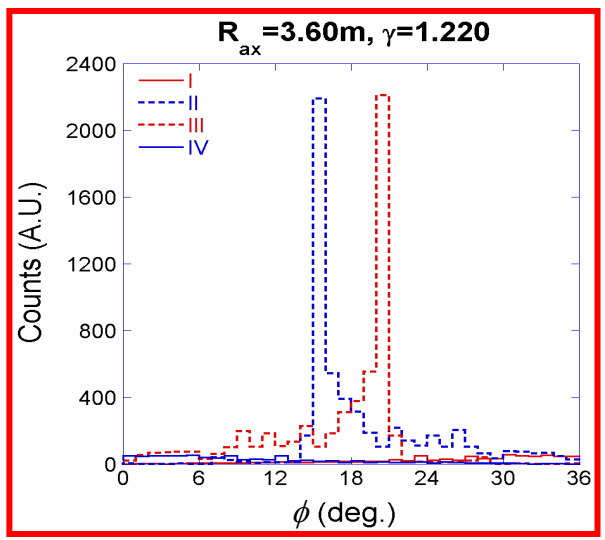

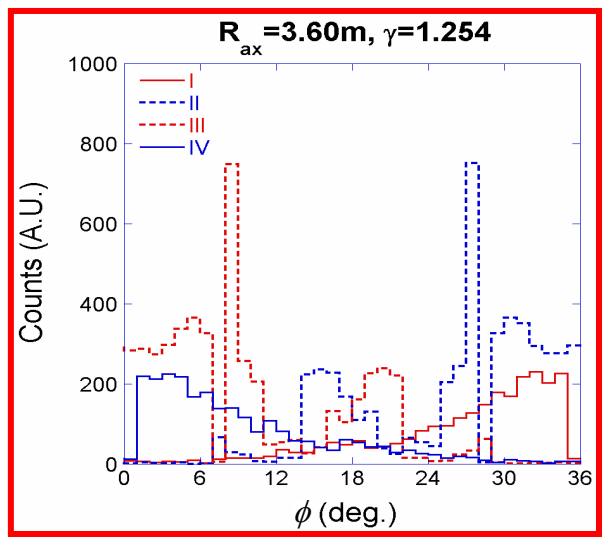

Images of Visible Emission Observed with the Cameras

Dependence of γ, R_{ax}=3.60m, B_q=100%

γ=1.259

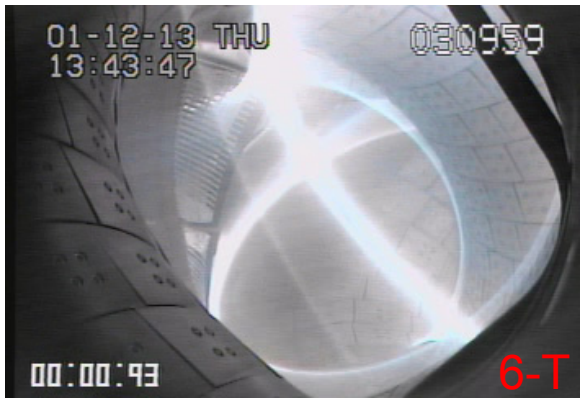

γ=1.262

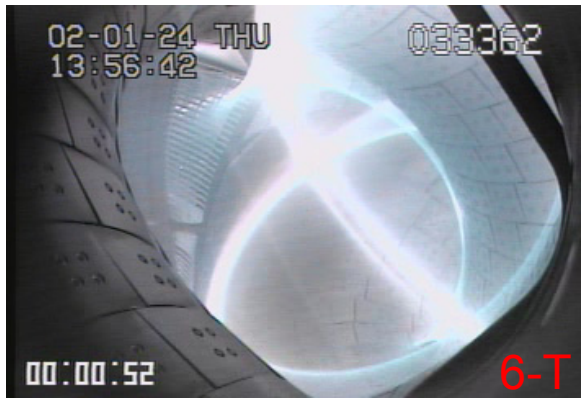

The area of the visible emission profile in the minor radius observed from a tangential port (6-T) increases in the coil pitch parameter (γ).

Images of the 3-D Plots of the Magnetic Field Lines

γ=1.259

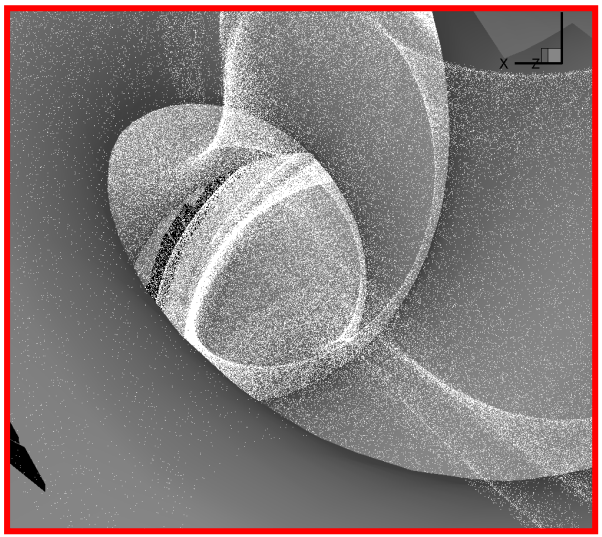

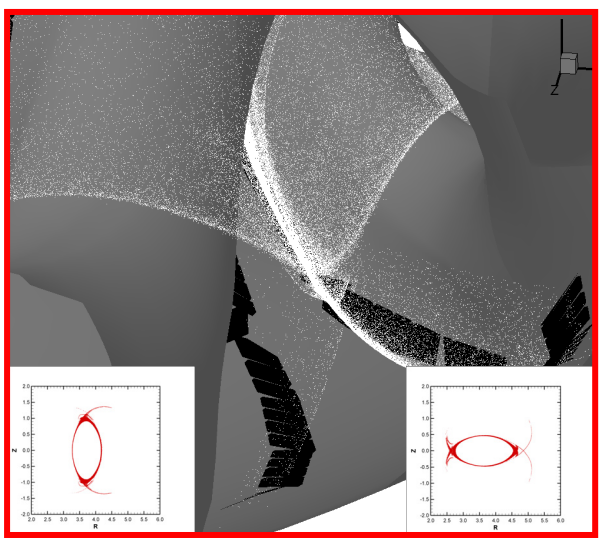

γ=1.262

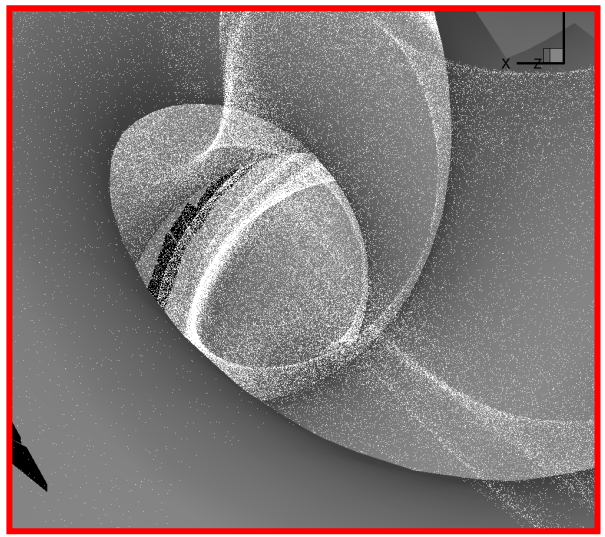

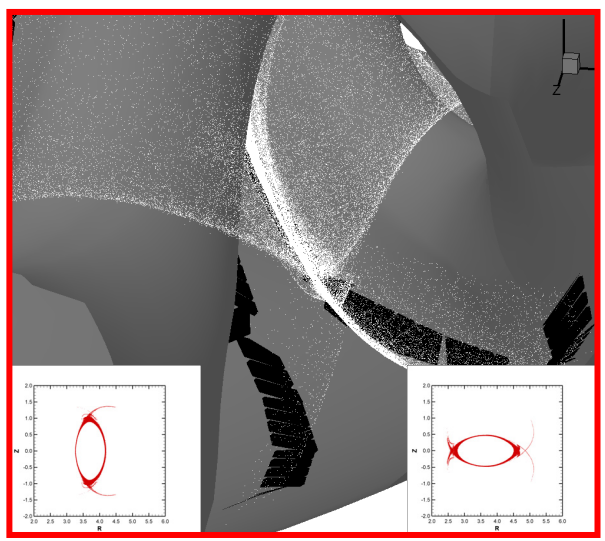

Toroidal and Poloidal Distribution of Strike Points

γ=1.259

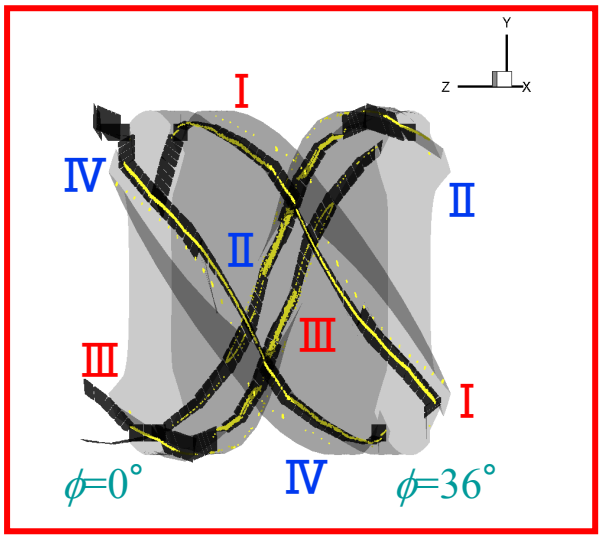

γ=1.262

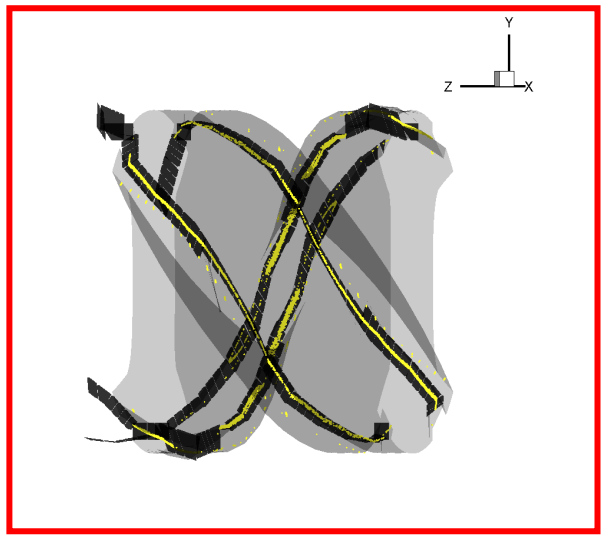

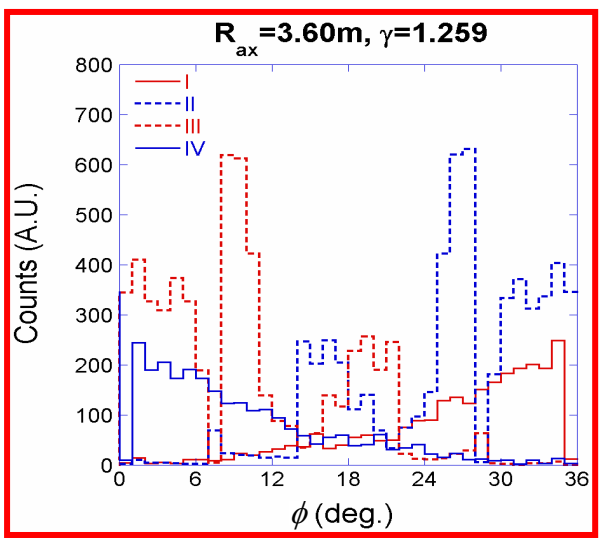

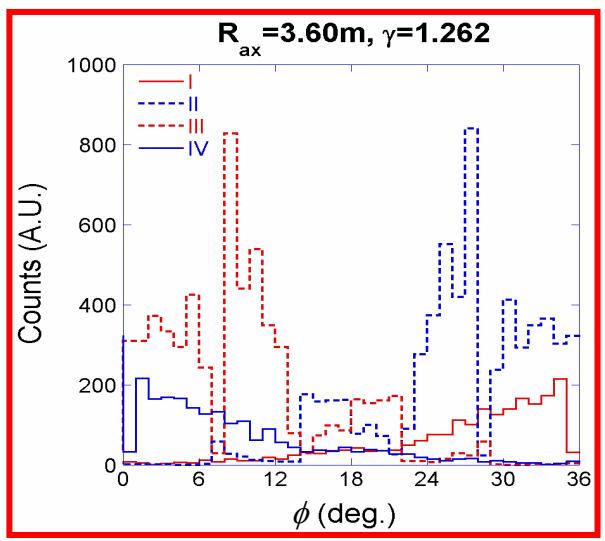

Images of Visible Emission Observed with the Cameras

Dependence of R_{ax}, γ=1.254, B_q=100%

R_{ax}=3.50m	R_{ax}=3.55m	R_{ax}=3.60m
		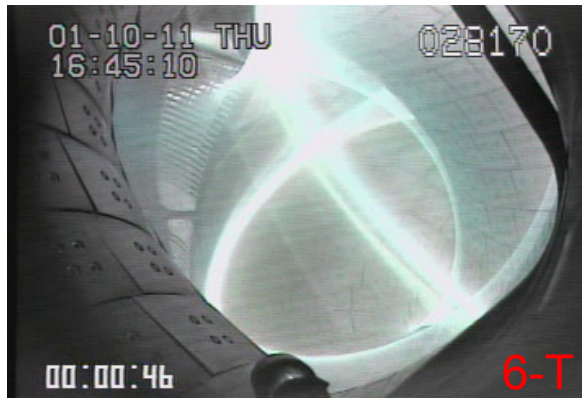
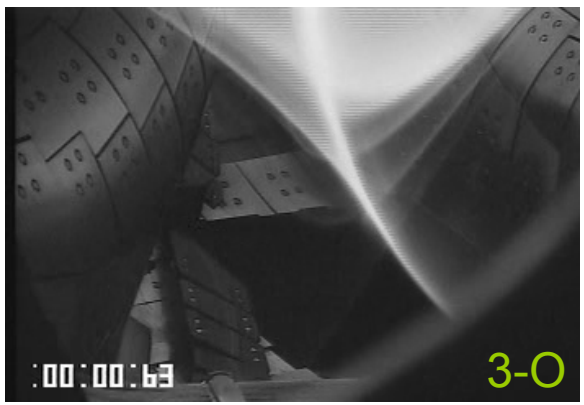	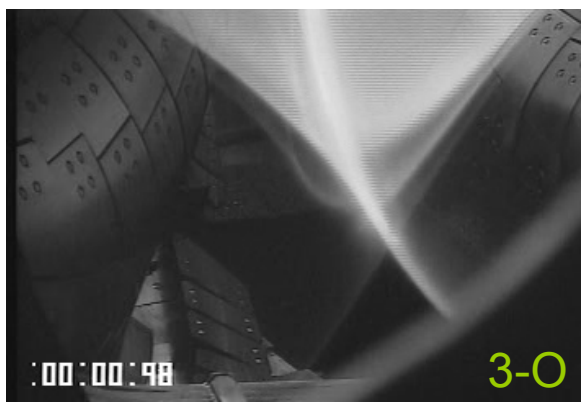	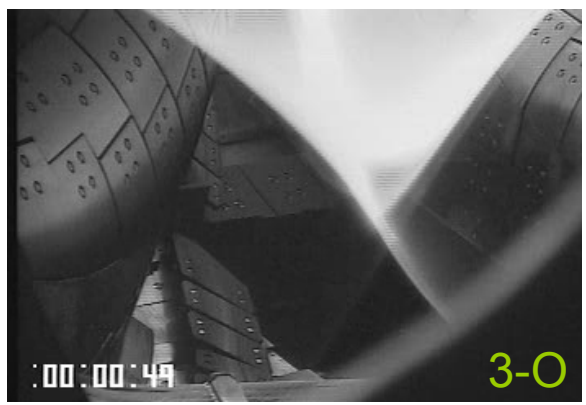

Transition of the bright area on the divertor legs from right to left side with the radial position of the magnetic axis (R_{ax}) is observed from an outer port (3-O).

Images of the 3-D Plots of the Magnetic Field Lines

R_{ax}=3.50m

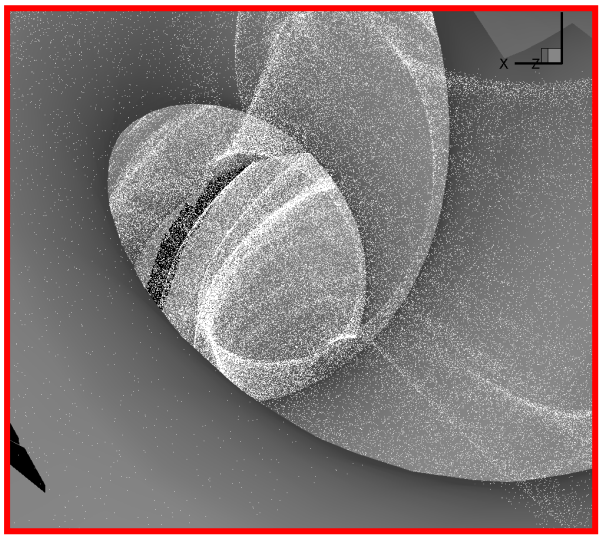

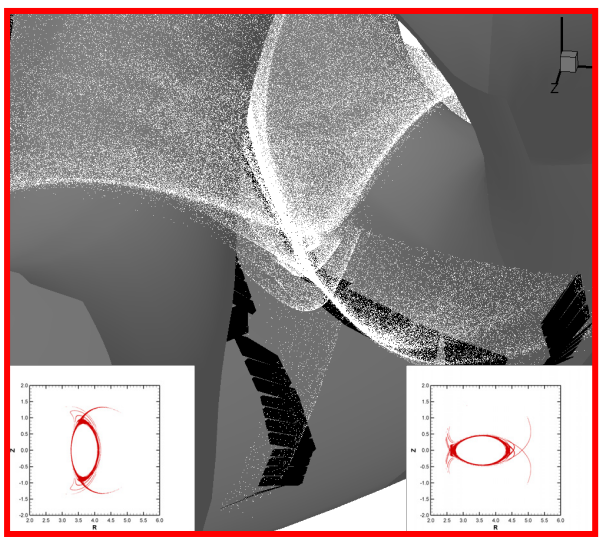

R_{ax}=3.55m

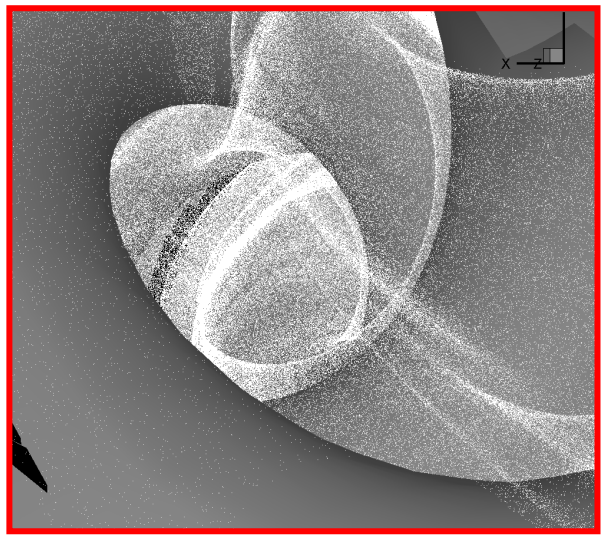

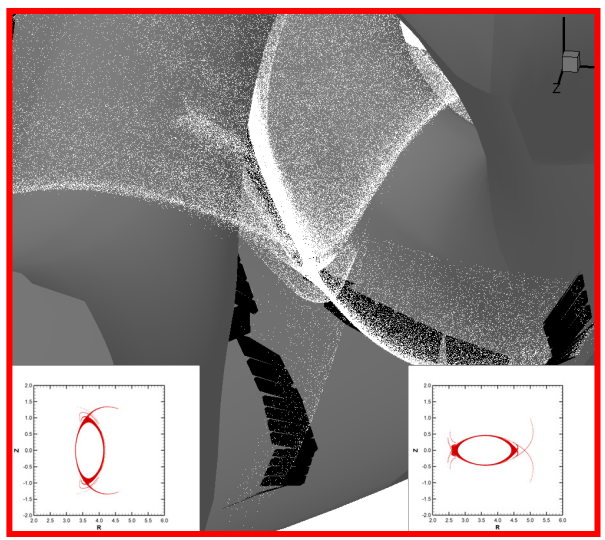

R_{ax}=3.60m

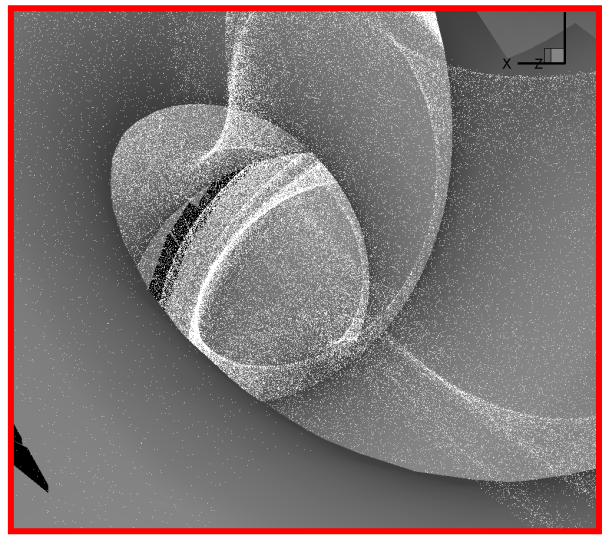

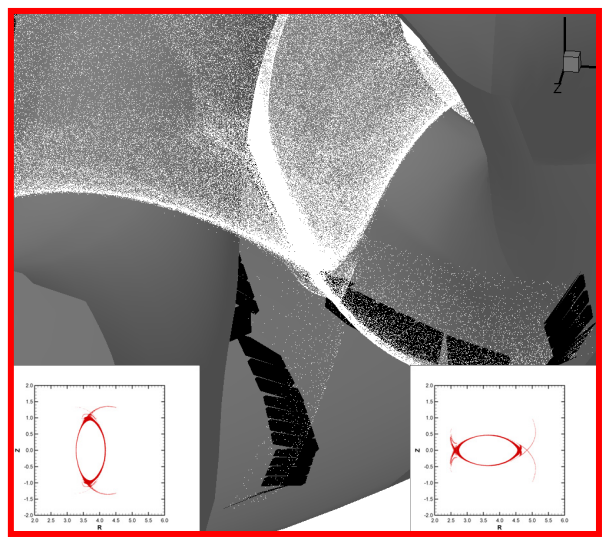

Toroidal and Poloidal Distribution of Strike Points

R_{ax}=3.50m

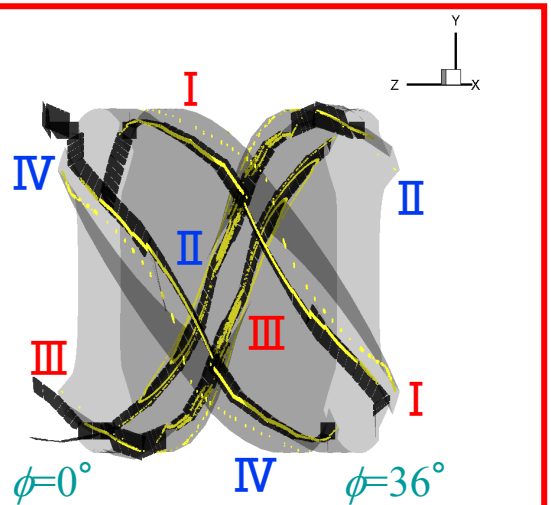

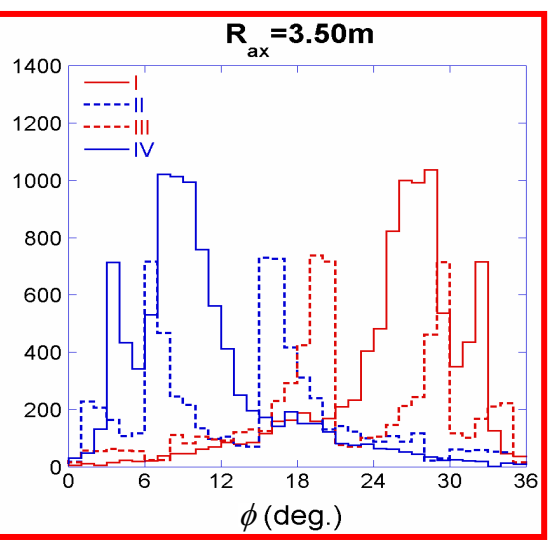

R_{ax}=3.55m

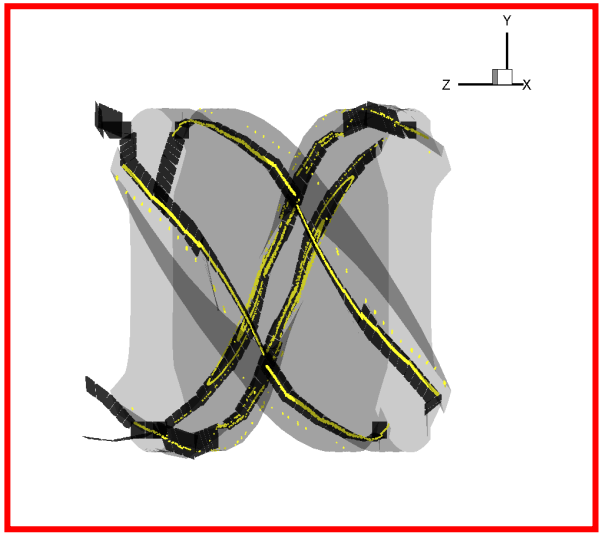

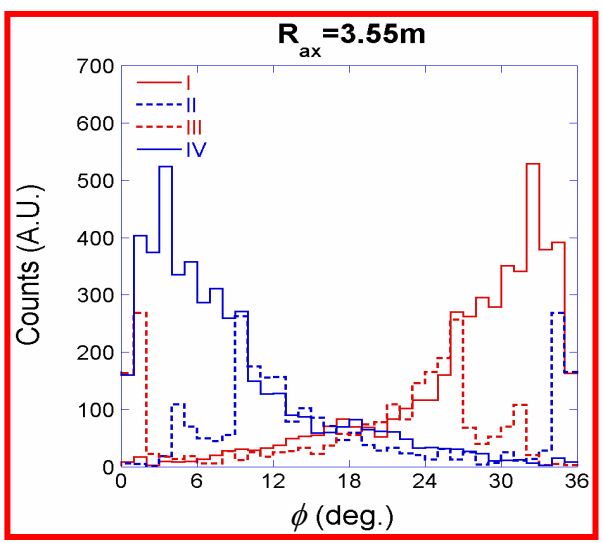

R_{ax}=3.60m

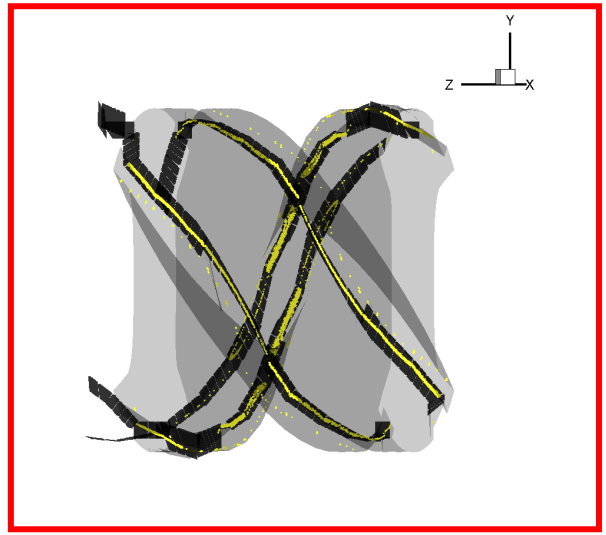

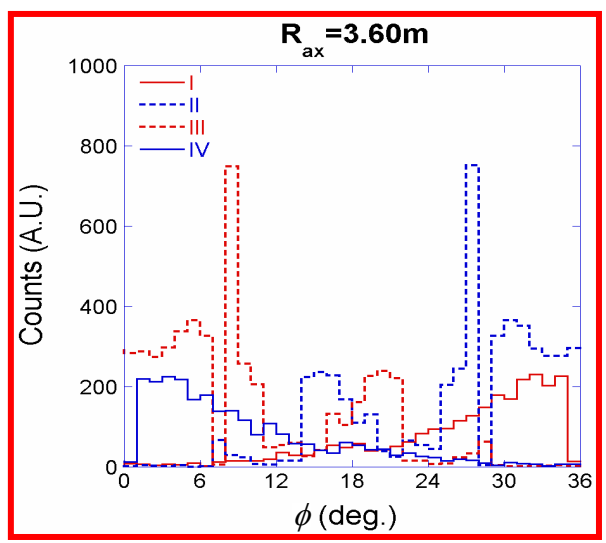

Images of Visible Emission Observed with the Cameras

Dependence of R_{ax}, γ=1.254, B_q=100%

R_{ax}=3.65m

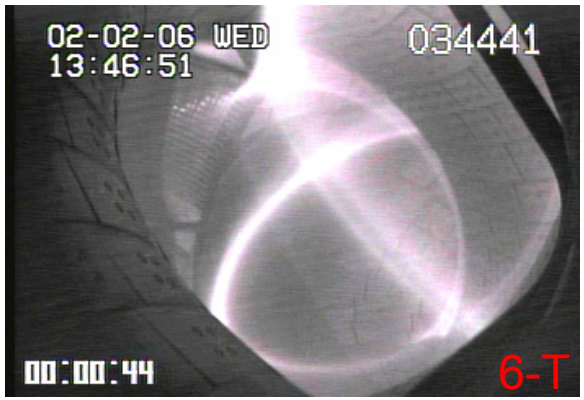

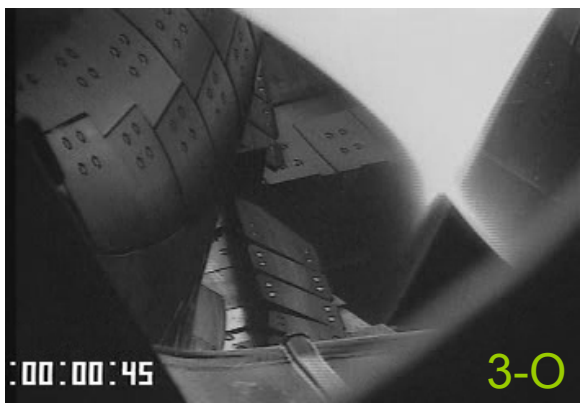

R_{ax}=3.70m

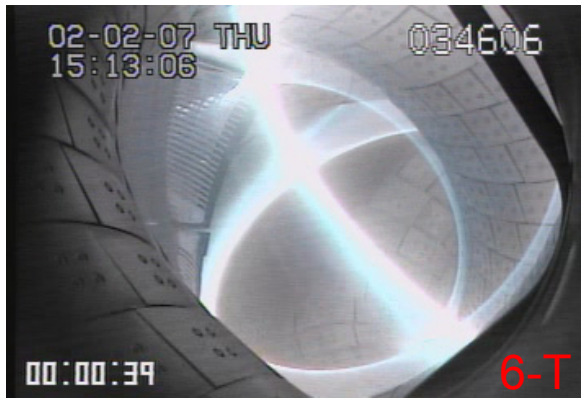

R_{ax}=3.75m

Transition of the bright area on the divertor legs from right to left side with the radial position of the magnetic axis (R_{ax}) is observed from an outer port (3-O).

Images of the 3-D Plots of the Magnetic Field Lines

R_{ax}=3.65m

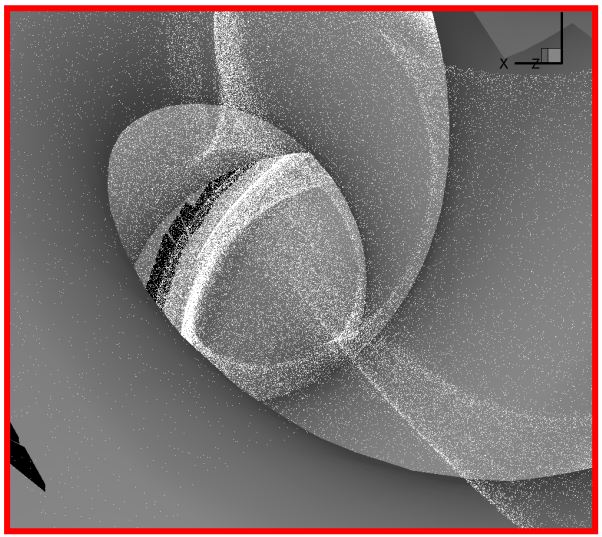

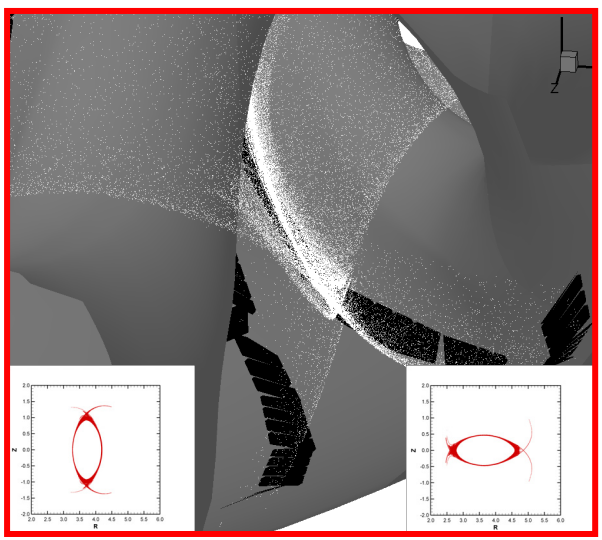

R_{ax}=3.70m

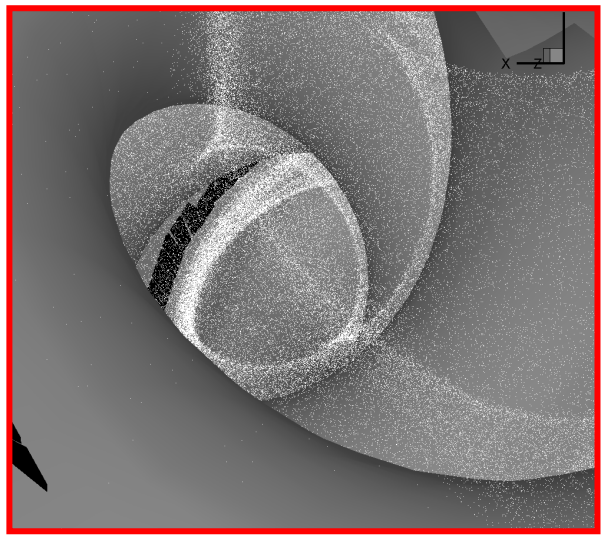

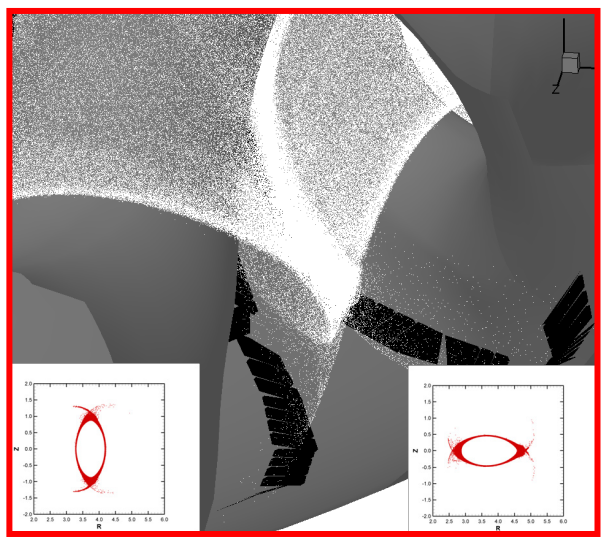

R_{ax}=3.75m

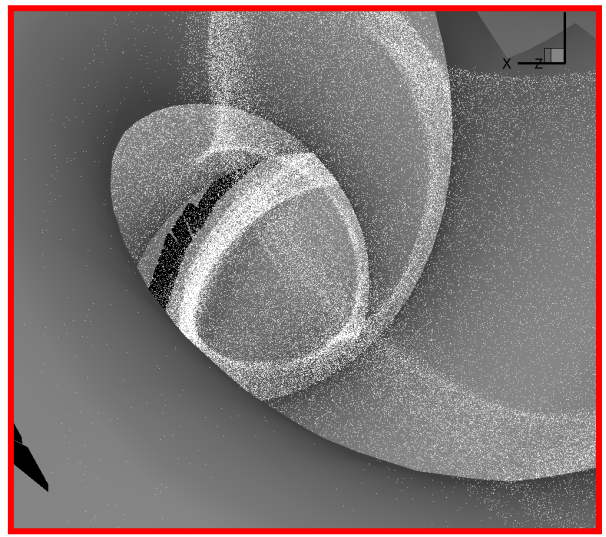

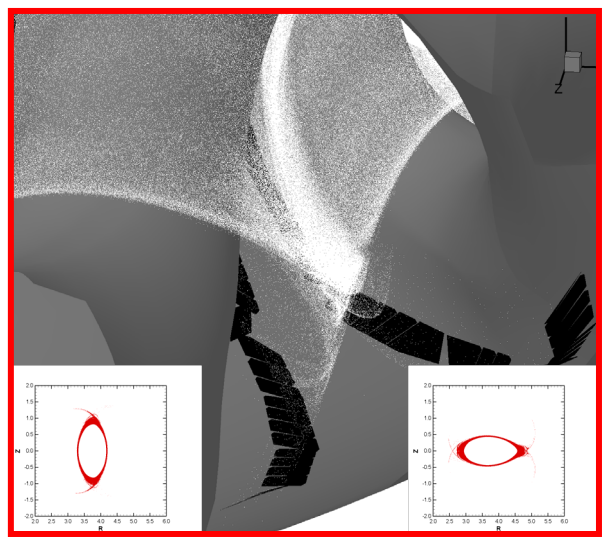

Toroidal and Poloidal Distribution of Strike Points

R_{ax}=3.65m

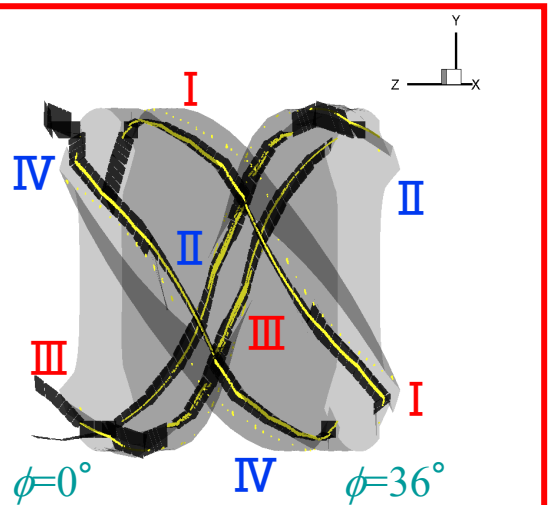

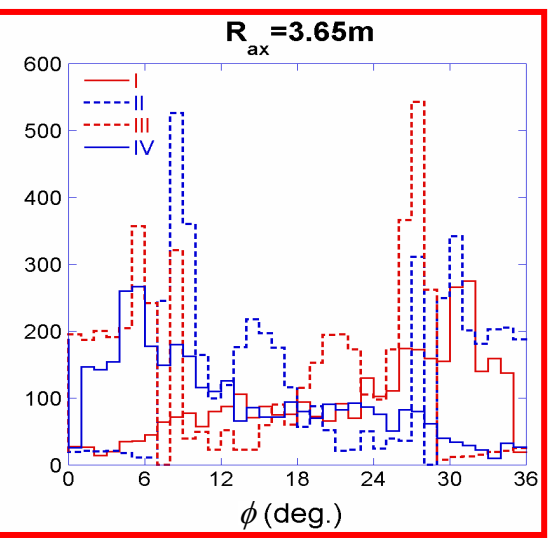

R_{ax}=3.70m

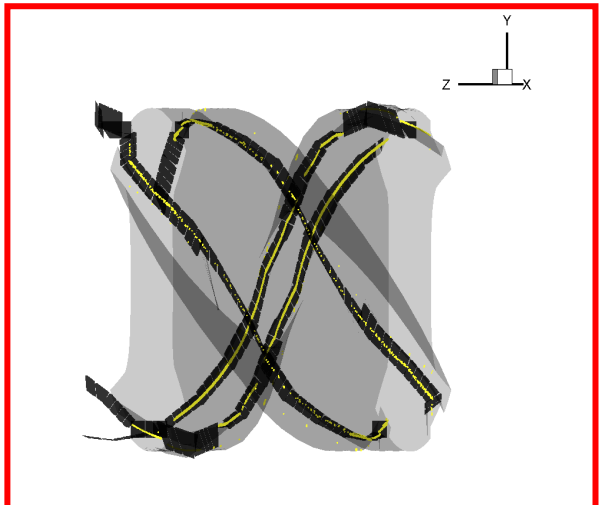

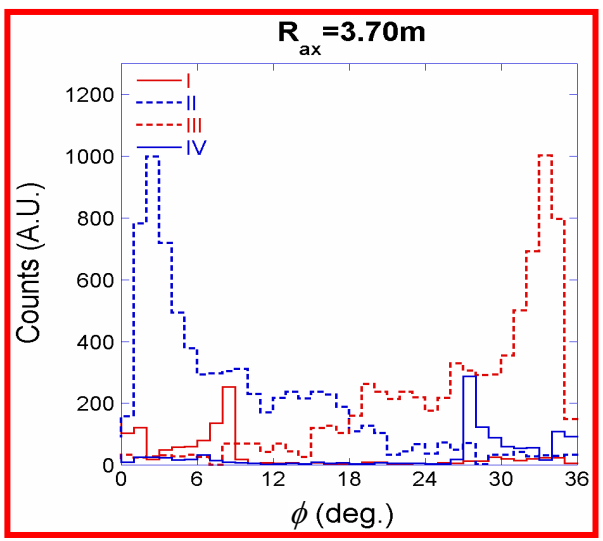

R_{ax}=3.75m

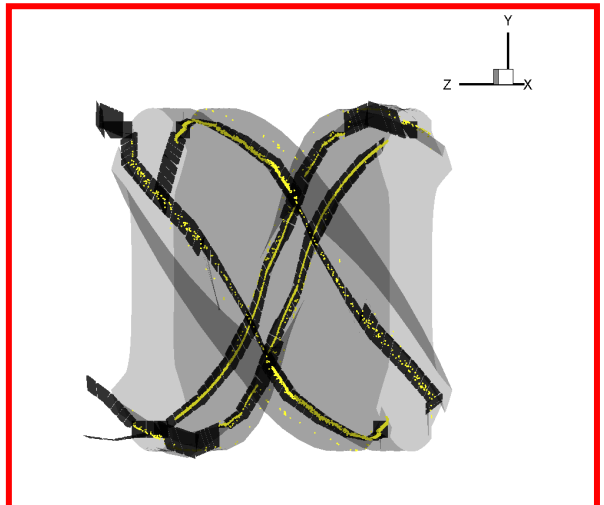

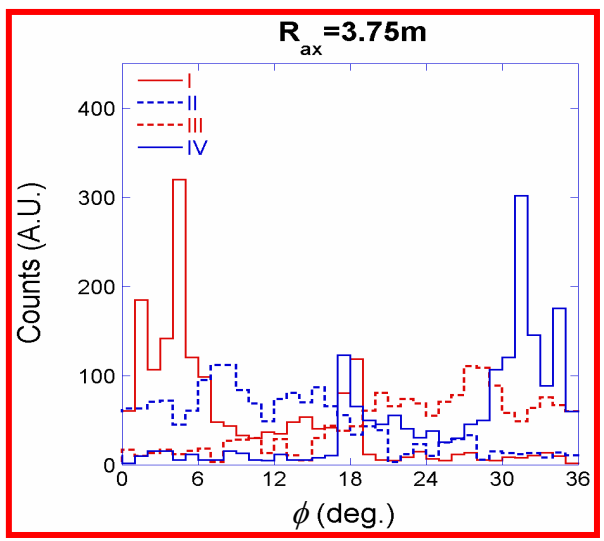

Images of Visible Emission Observed with the Cameras

Dependence of R_{ax}, γ=1.254, B_q=100%

R_{ax}=3.80m

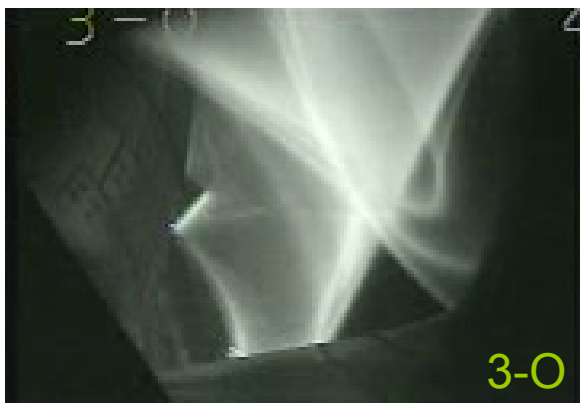

R_{ax}=3.90m

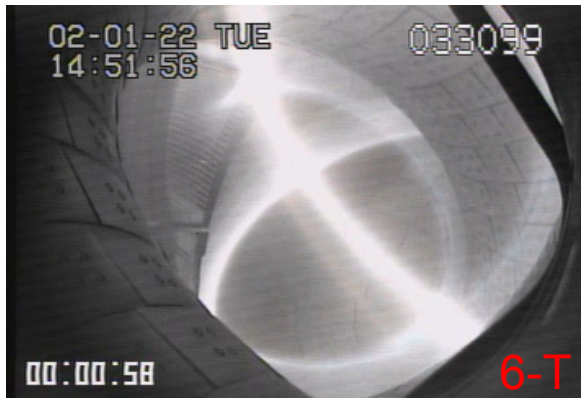

R_{ax}=4.05m

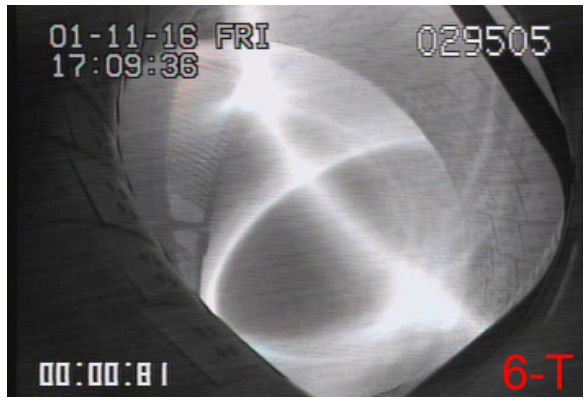

Transition of the bright area on the divertor legs from right to left side with the radial position of the magnetic axis (R_{ax}) is observed from an outer port (3-O).

Images of the 3-D Plots of the Magnetic Field Lines

R_{ax}=3.80m

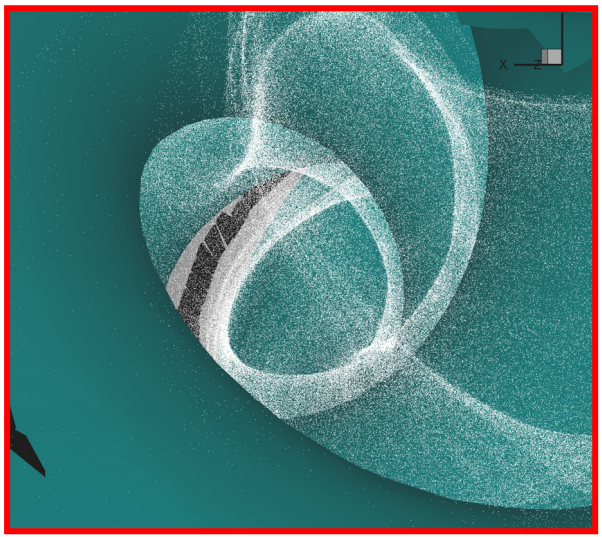

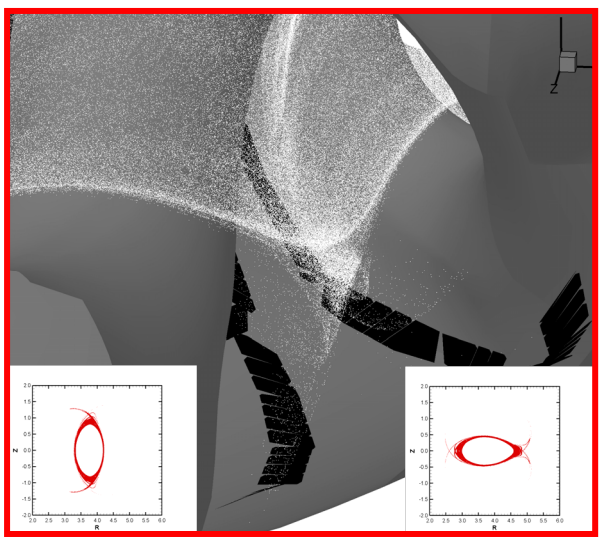

R_{ax}=3.90m

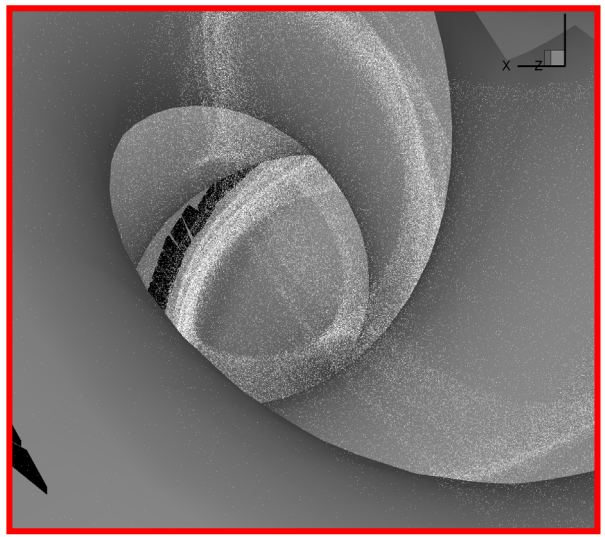

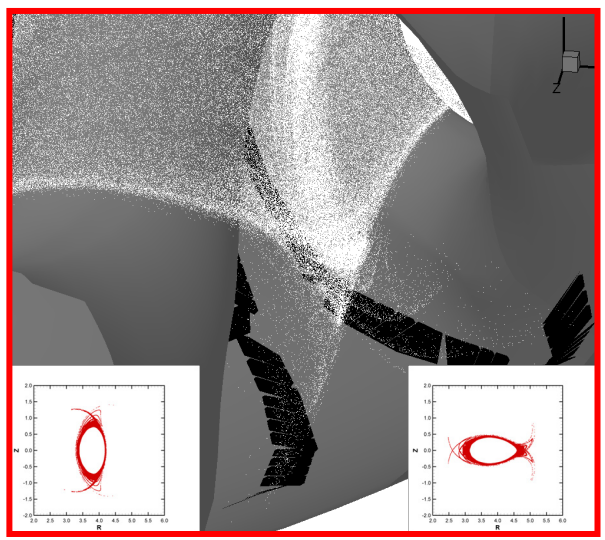

R_{ax}=4.05m

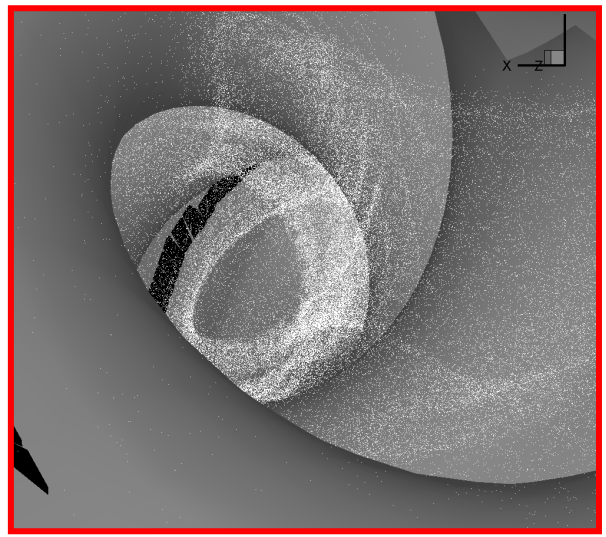

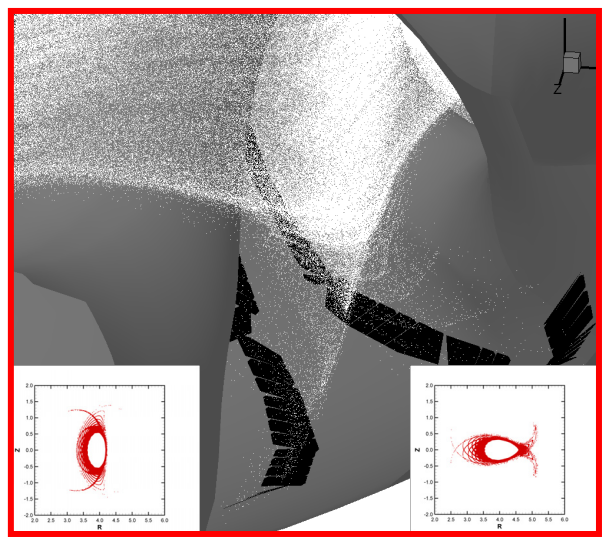

Toroidal and Poloidal Distribution of Strike Points

R_{ax}=3.80m

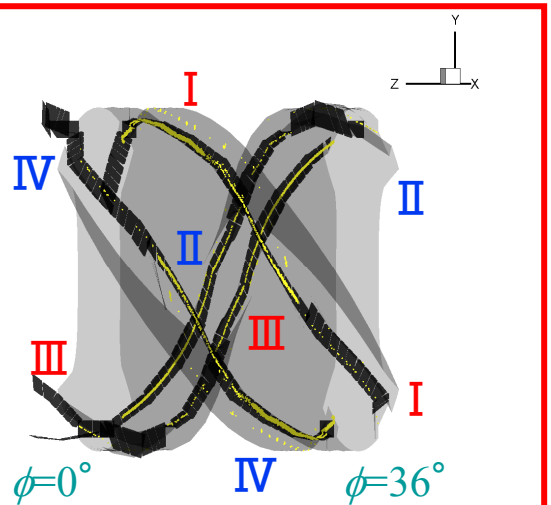

R_{ax}=3.90m

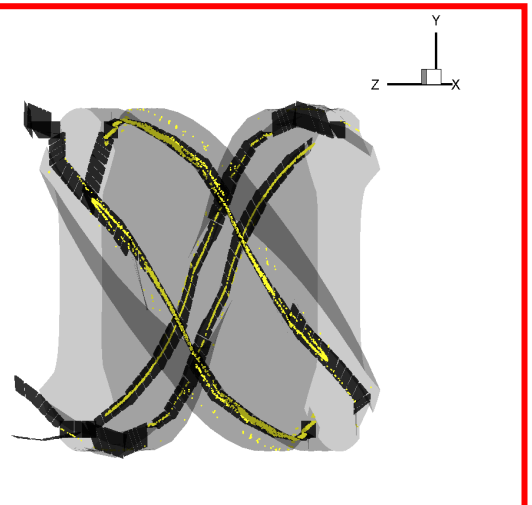

R_{ax}=4.05m

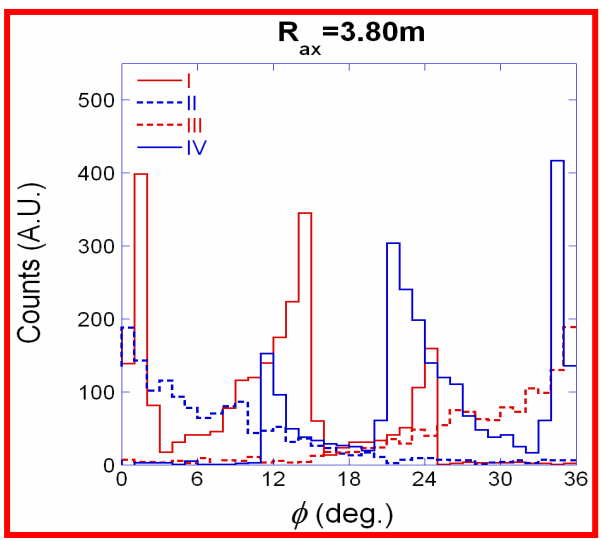

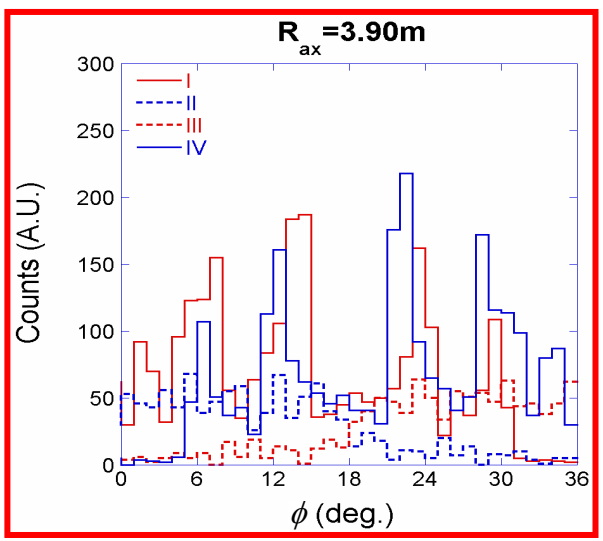

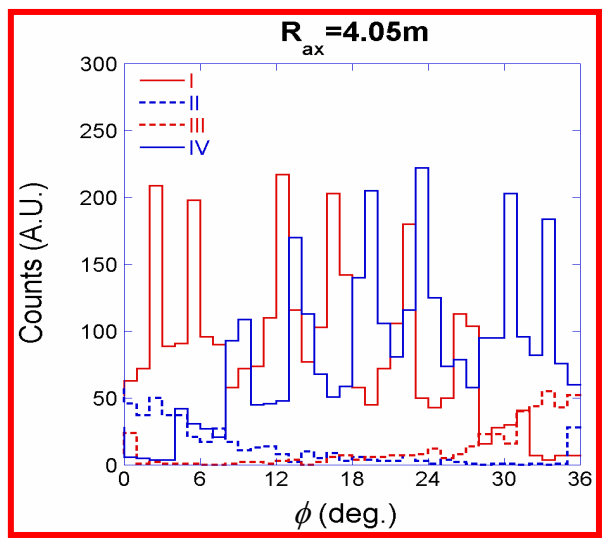

Images of Visible Emission Observed with the Cameras

Dependence of B_q, R_{ax}=3.60m, γ=1.254

B_Q=-200% B_Q=-150% B_Q= -100%

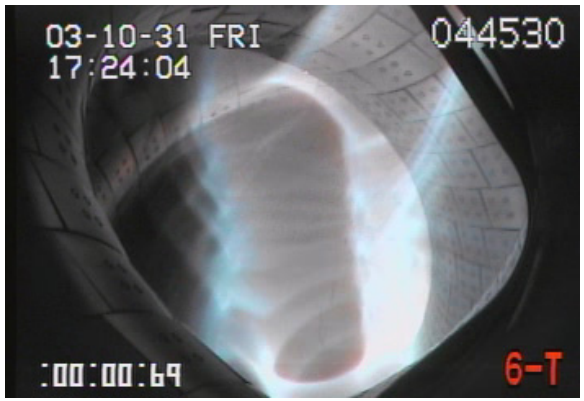

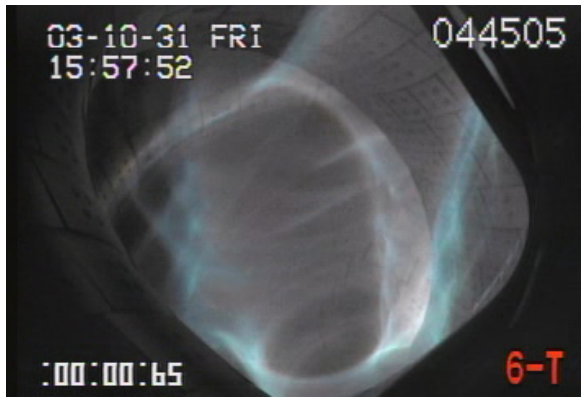

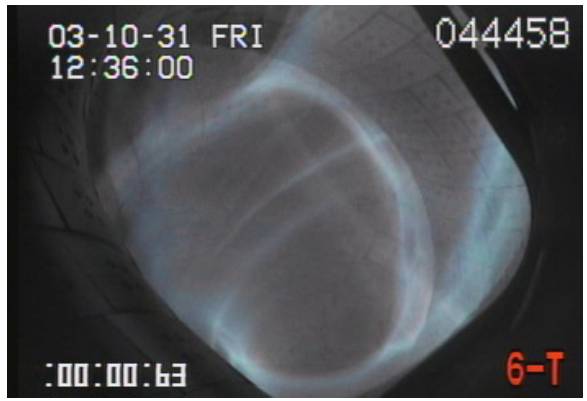

Deformation of the profile of the visible emission is observed from a tangential port (6-T) with the change of the quadrupole magnetic component (B_q).

Images of the 3-D Plots of the Magnetic Field Lines

B_Q=-200%

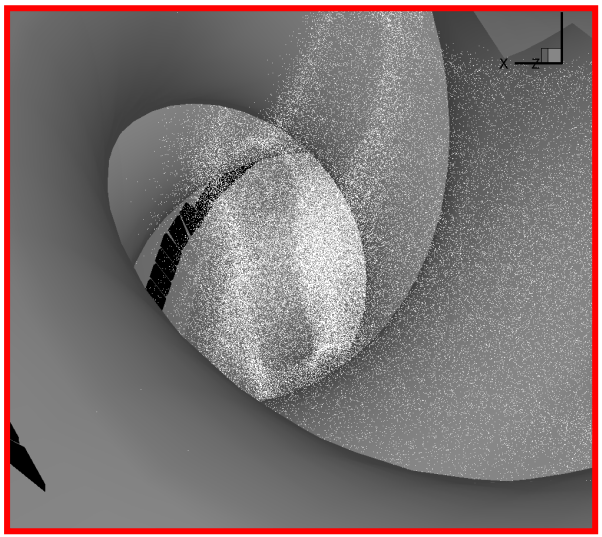

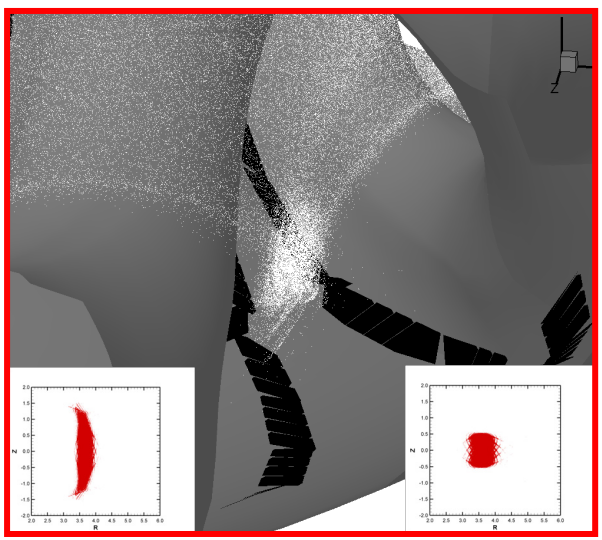

B_Q=-150%

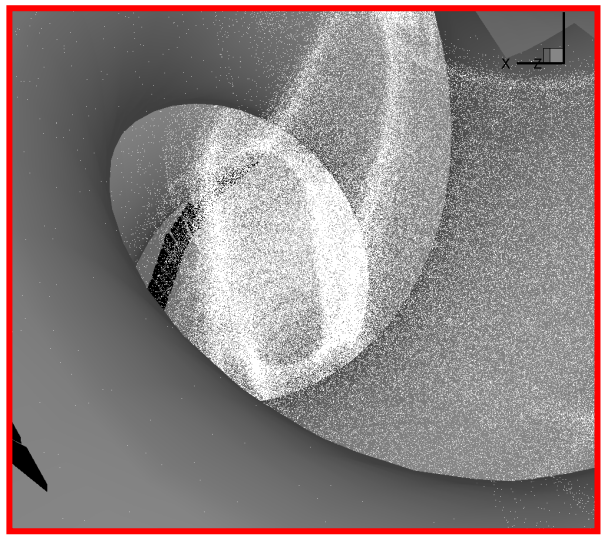

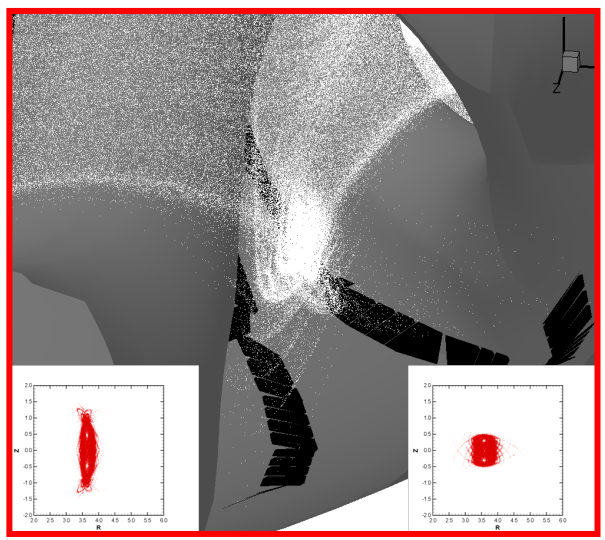

B_Q=-100%

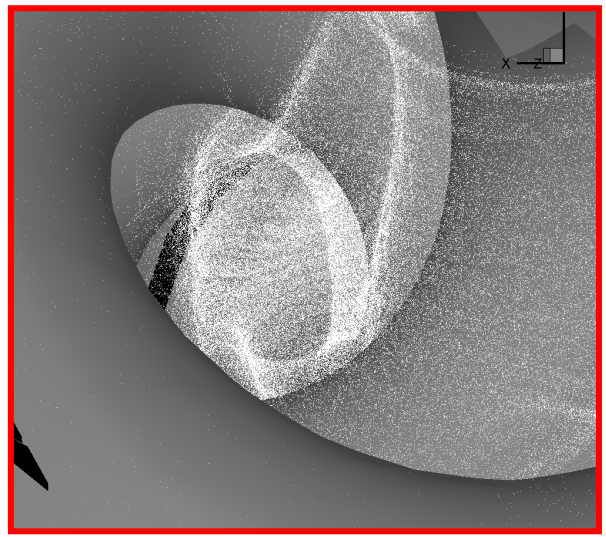

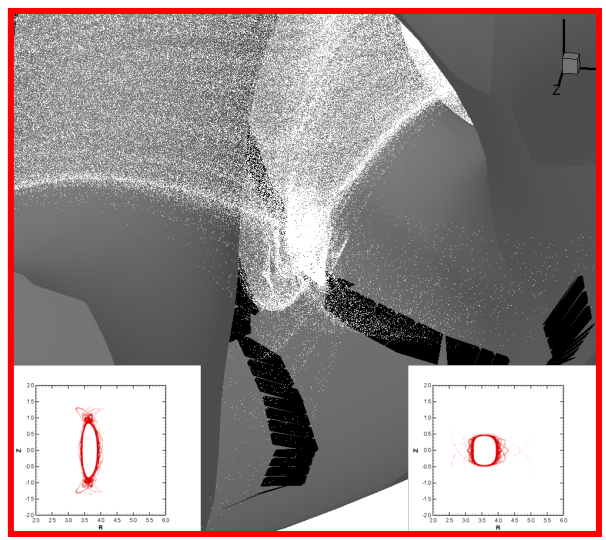

Toroidal and Poloidal Distribution of Strike Points

B_Q=-200%

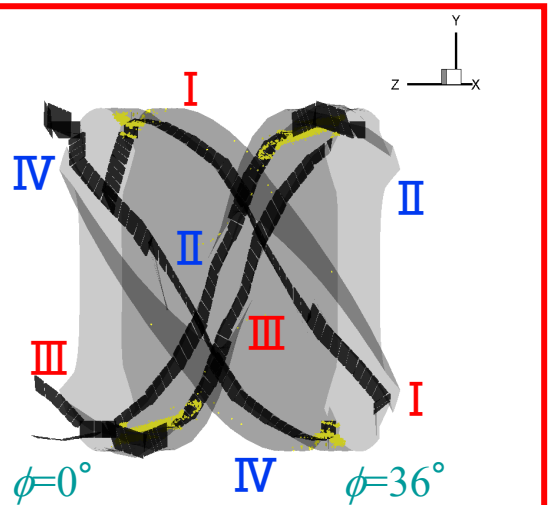

B_Q=-150%

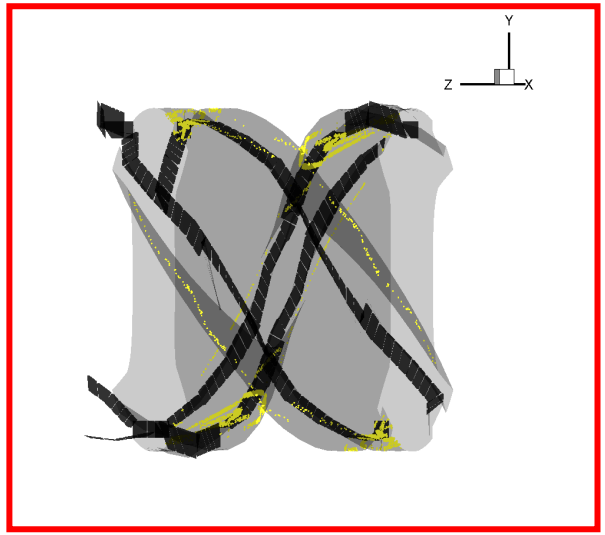

B_Q=-100%

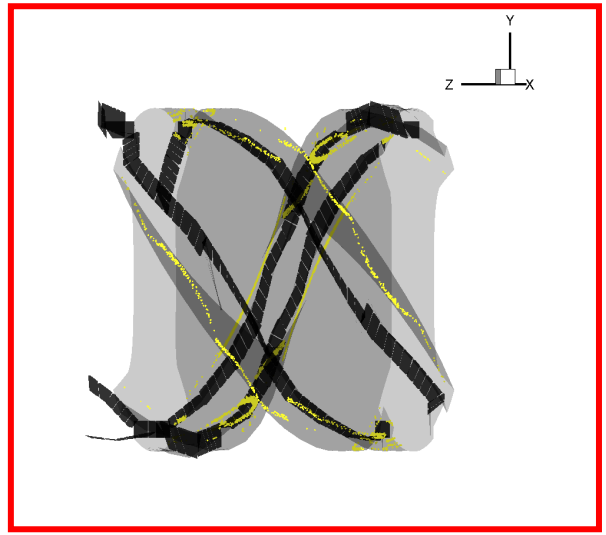

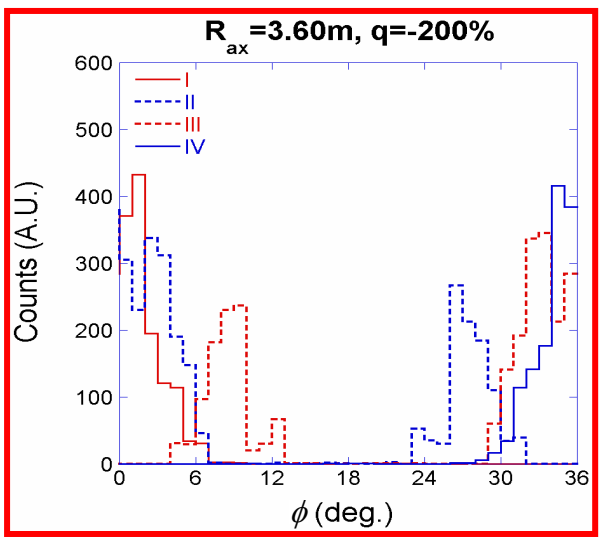

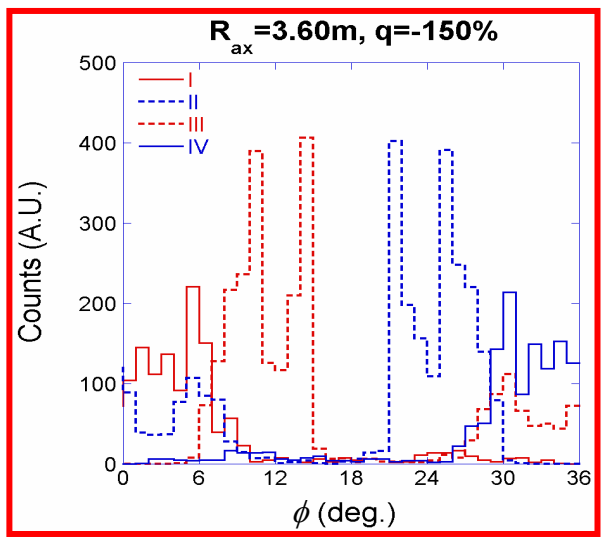

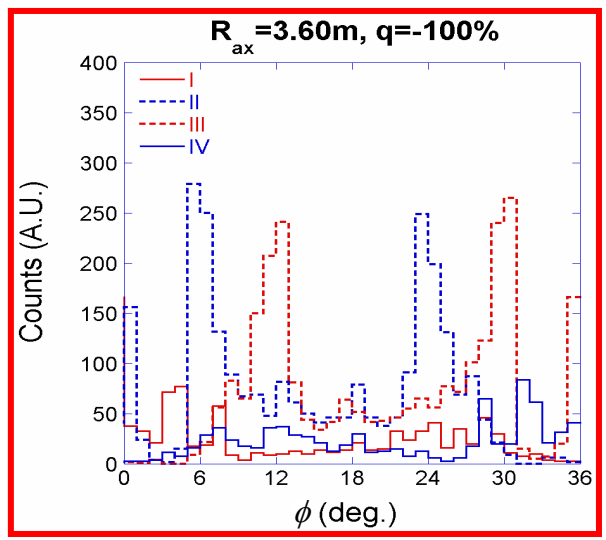

Images of Visible Emission Observed with the Cameras

Dependence of B_q, R_{ax}=3.60m, γ=1.254

B_Q=-50%	B_Q=0%	B_Q=72%
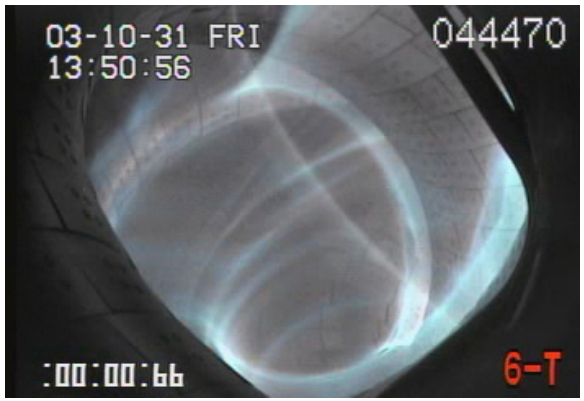	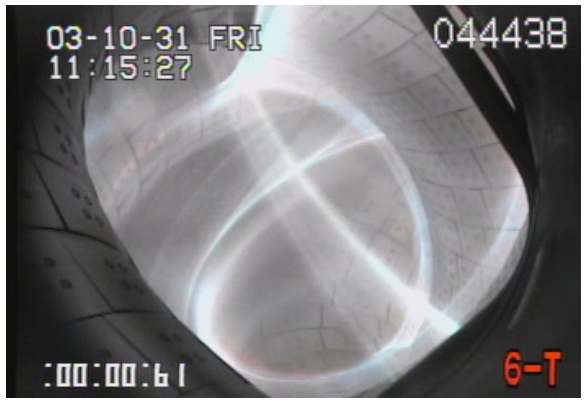	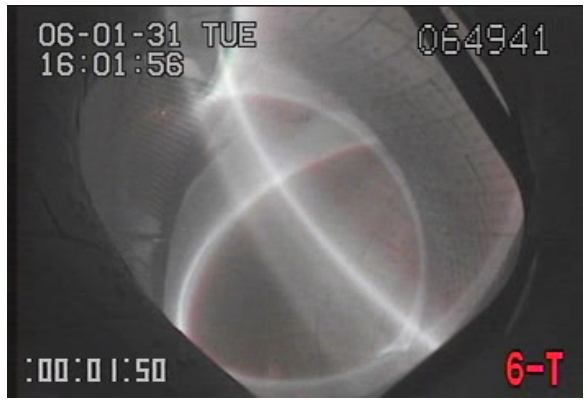
	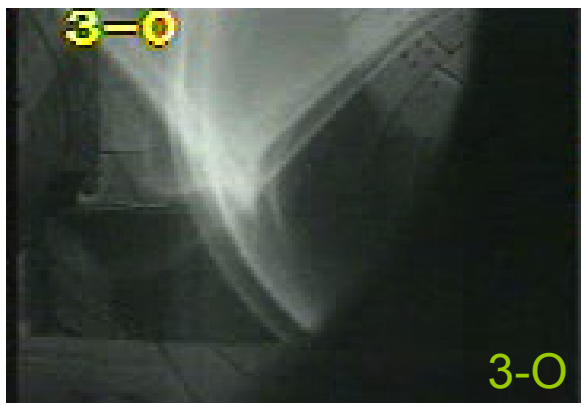	

Deformation of the profile of the visible emission is observed from a tangential port (6-T) with the change of the quadrupole magnetic component (B_q).

Images of the 3-D Plots of the Magnetic Field Lines

B_Q=-50%

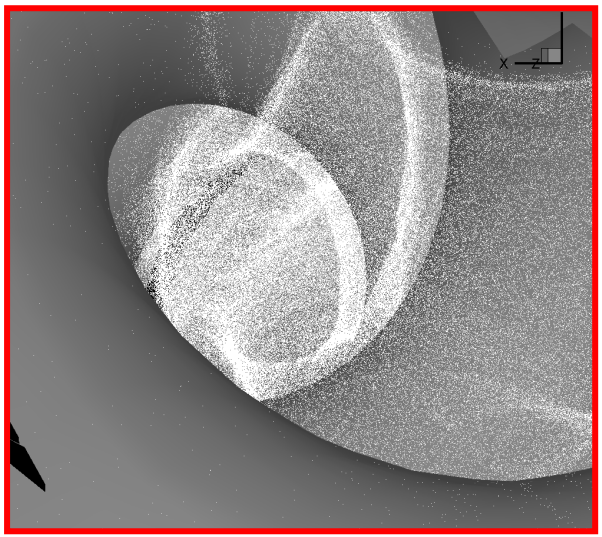

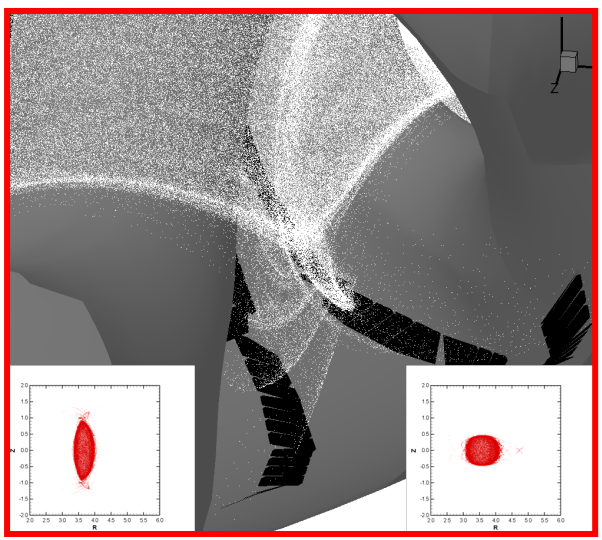

B_Q=0%

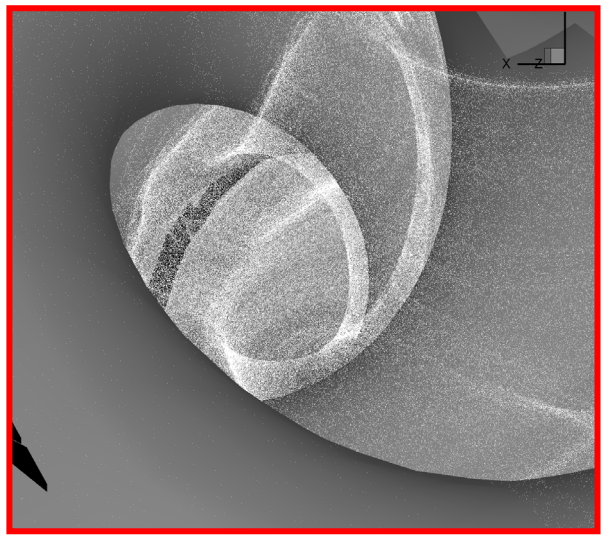

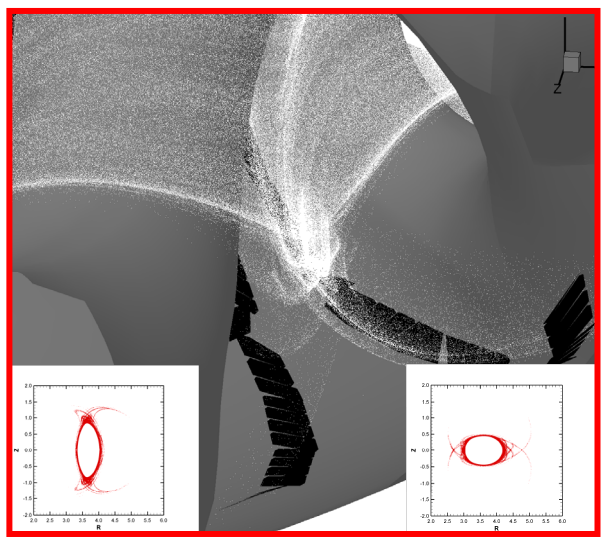

B_Q=72%

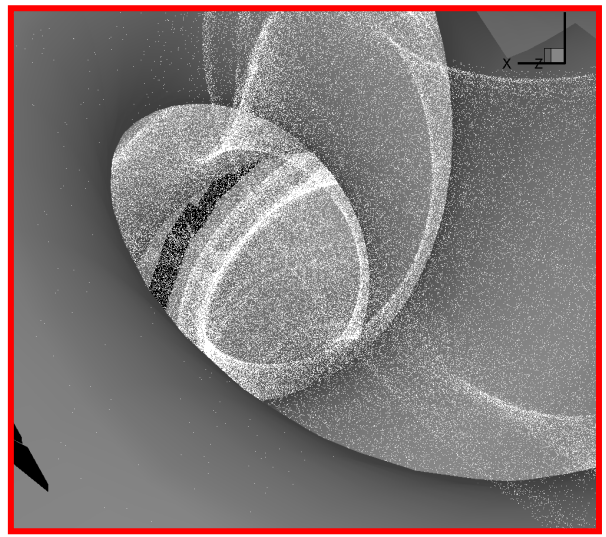

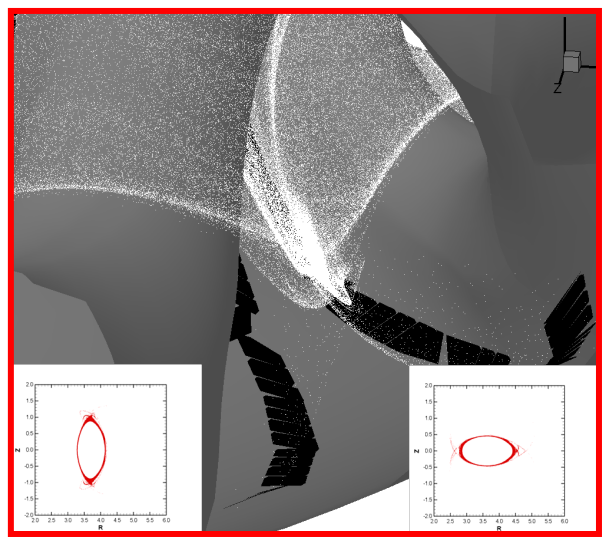

Toroidal and Poloidal Distribution of Strike Points

B_Q=-50%

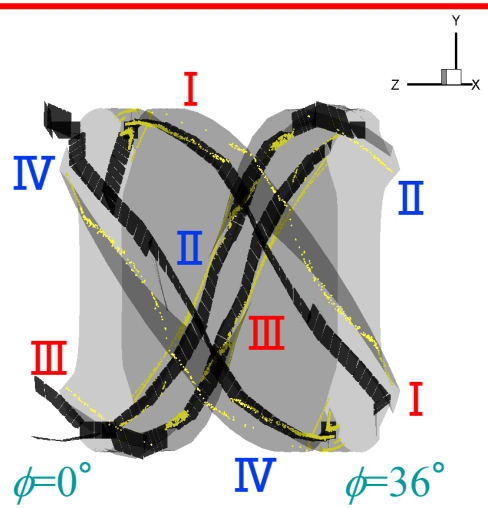

B_Q=0%

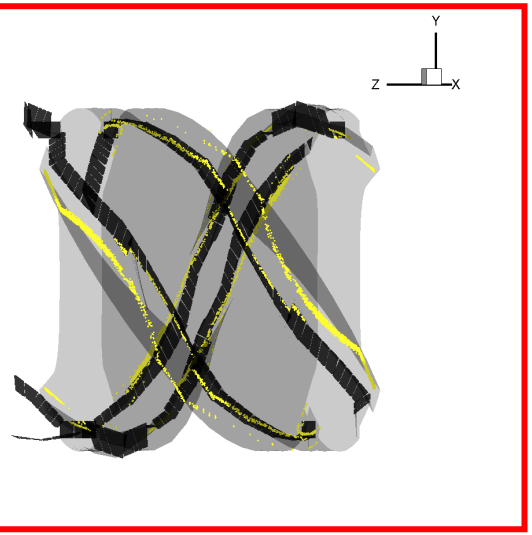

B_Q=72%

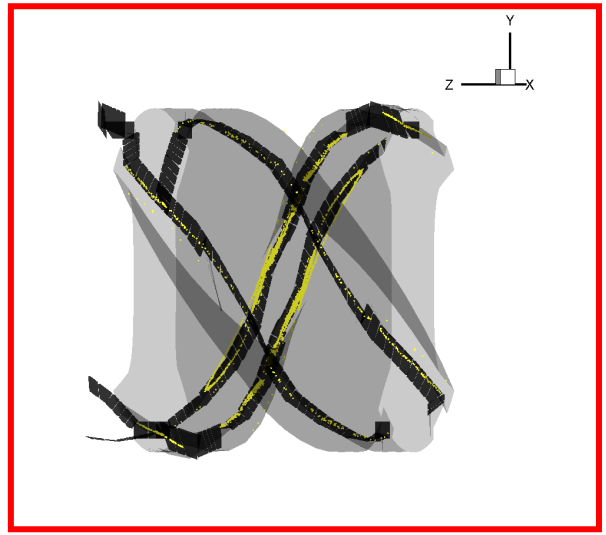

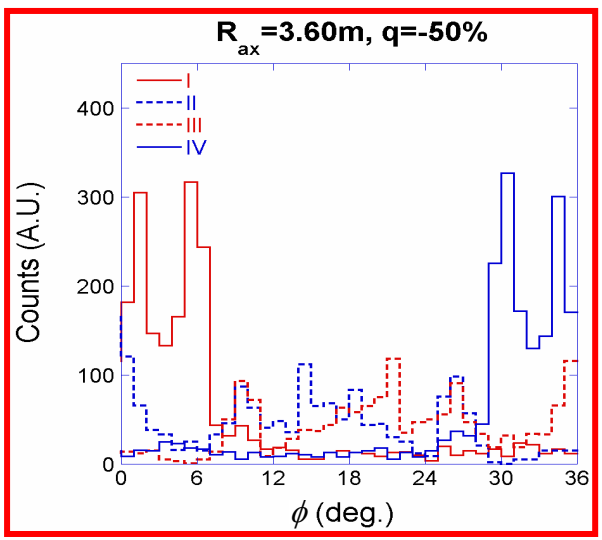

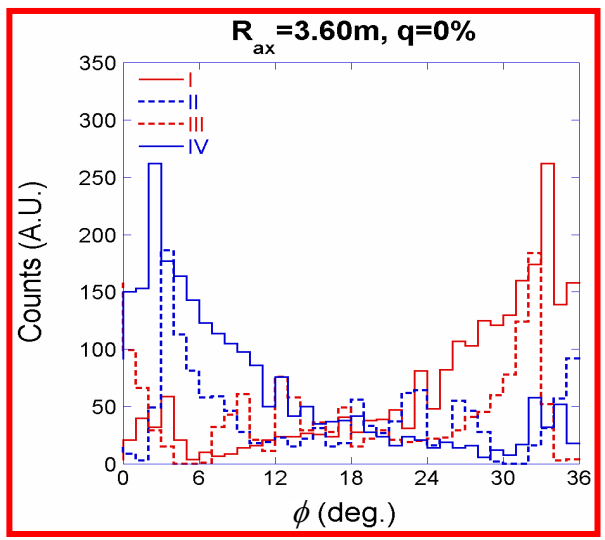

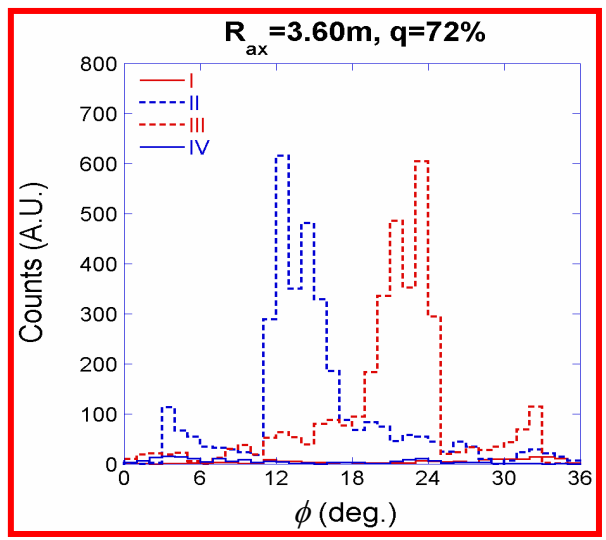

Images of Visible Emission Observed with the Cameras

Dependence of B_q, R_{ax}=3.60m, γ=1.254

B_Q=100%	B_Q=150%	B_Q=200%
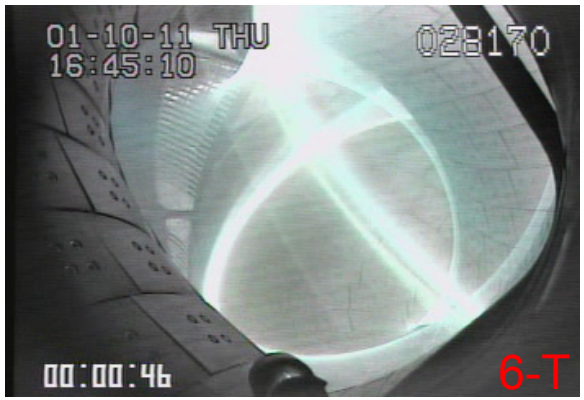	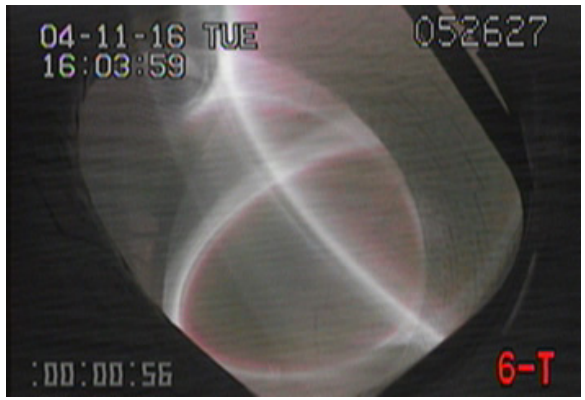	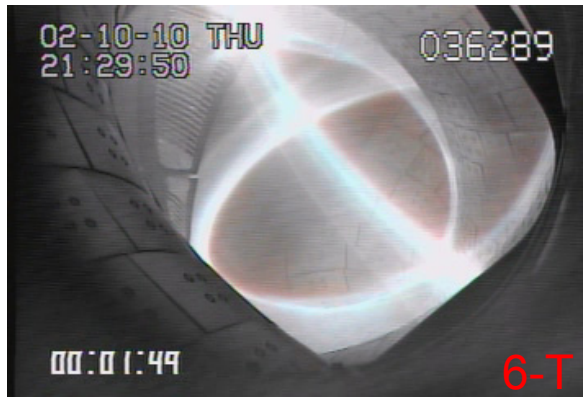
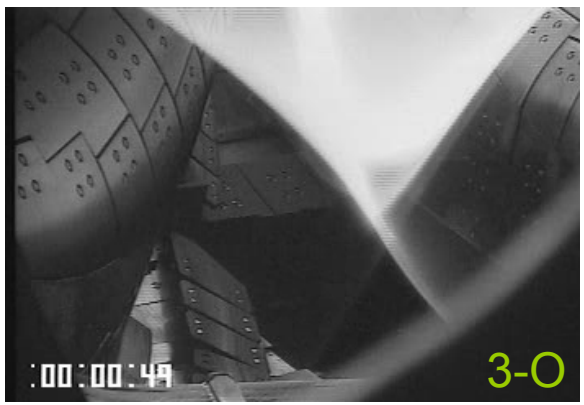	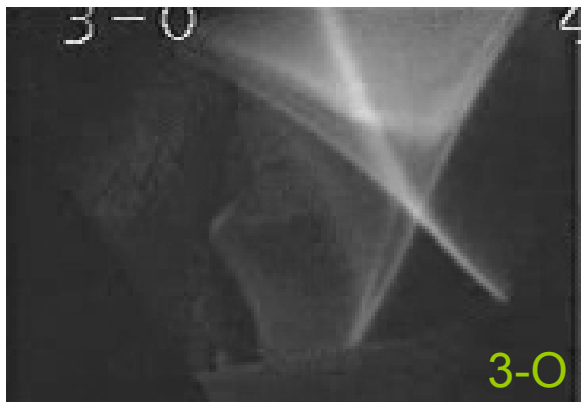	

Deformation of the profile of the visible emission is observed from a tangential port (6-T) with the change of the quadrupole magnetic component (B_q).

Images of the 3-D Plots of the Magnetic Field Lines

B_Q=100%

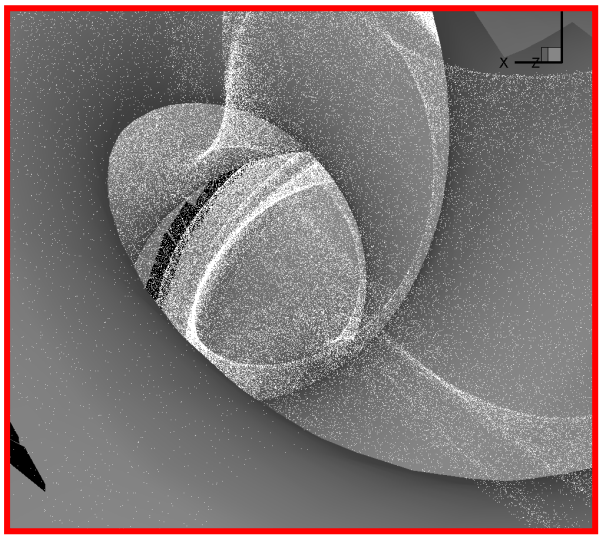

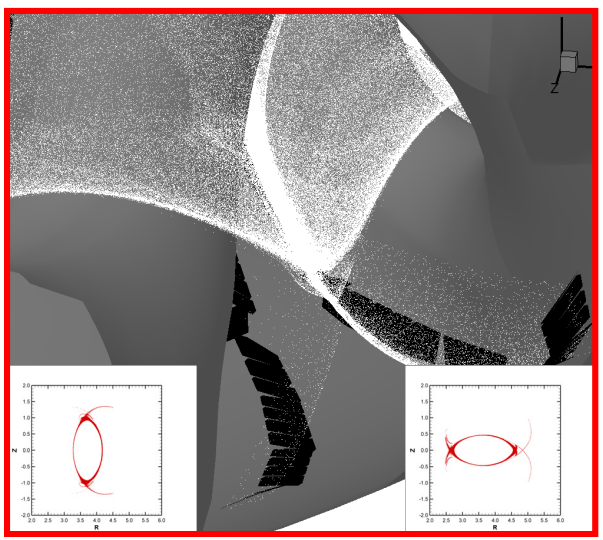

B_Q=150%

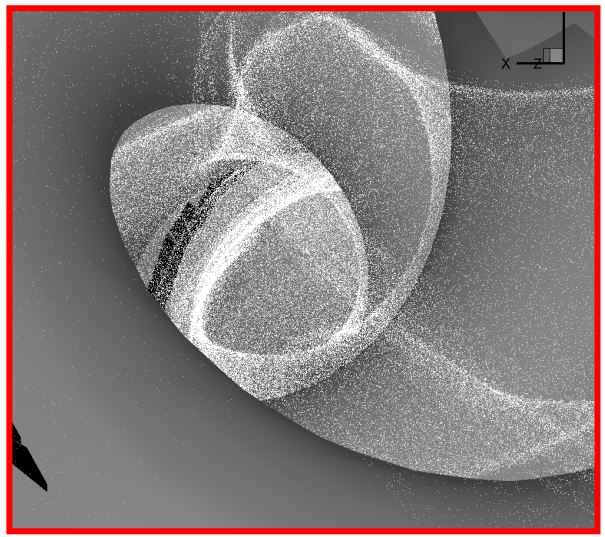

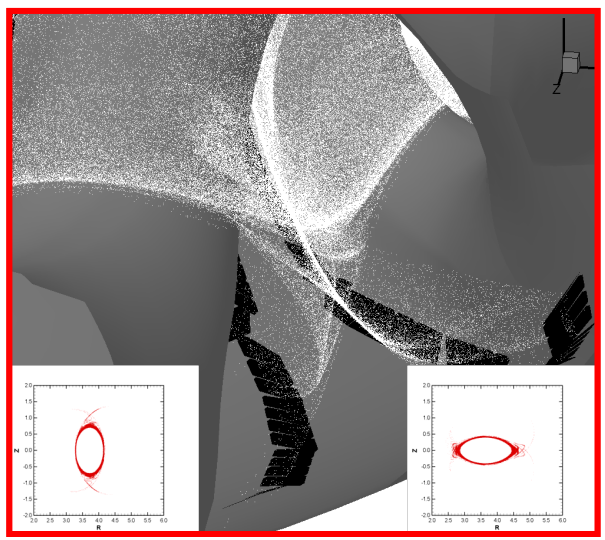

B_Q=200%

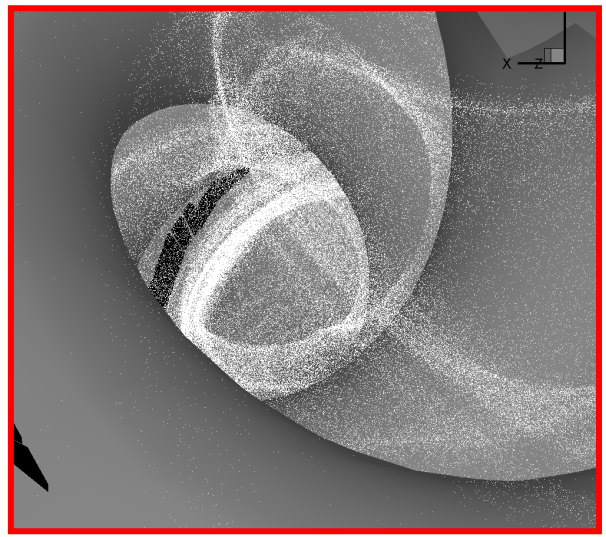

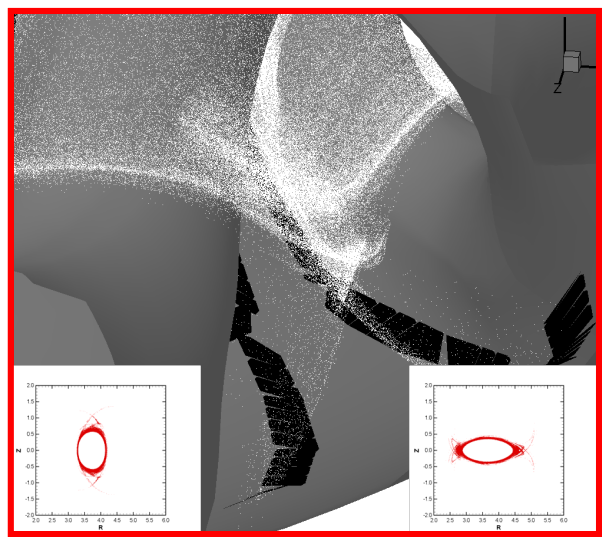

Toroidal and Poloidal Distribution of Strike Points

B_Q=100%

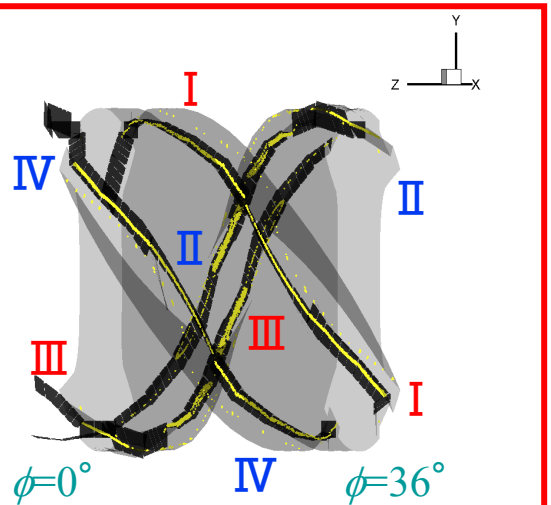

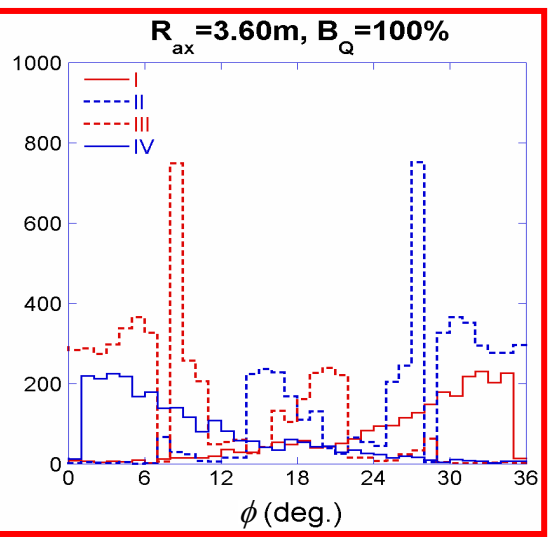

B_Q=150%

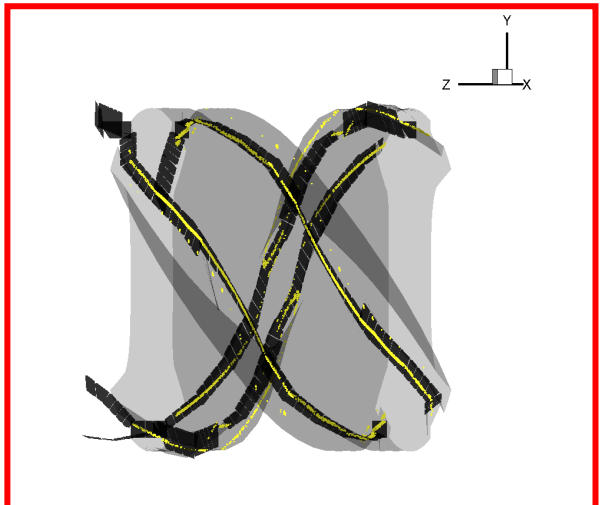

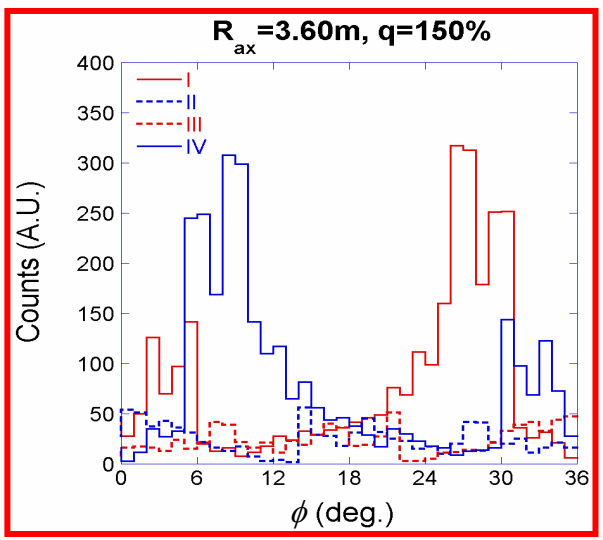

B_Q=200%

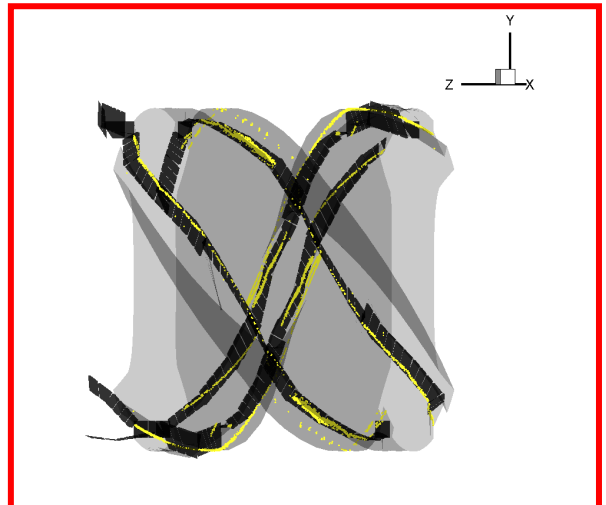

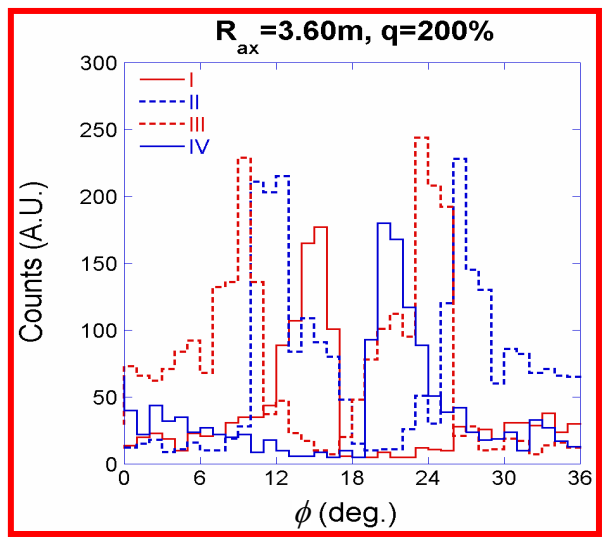

Dependence of N_{Div}/N_{Total} on the parameters (R_{ax}, γ, B_q)

N_{Div} : The number of the calculated strike points locating on divertor plates

N_{Total} : Total number of the calculated strike points

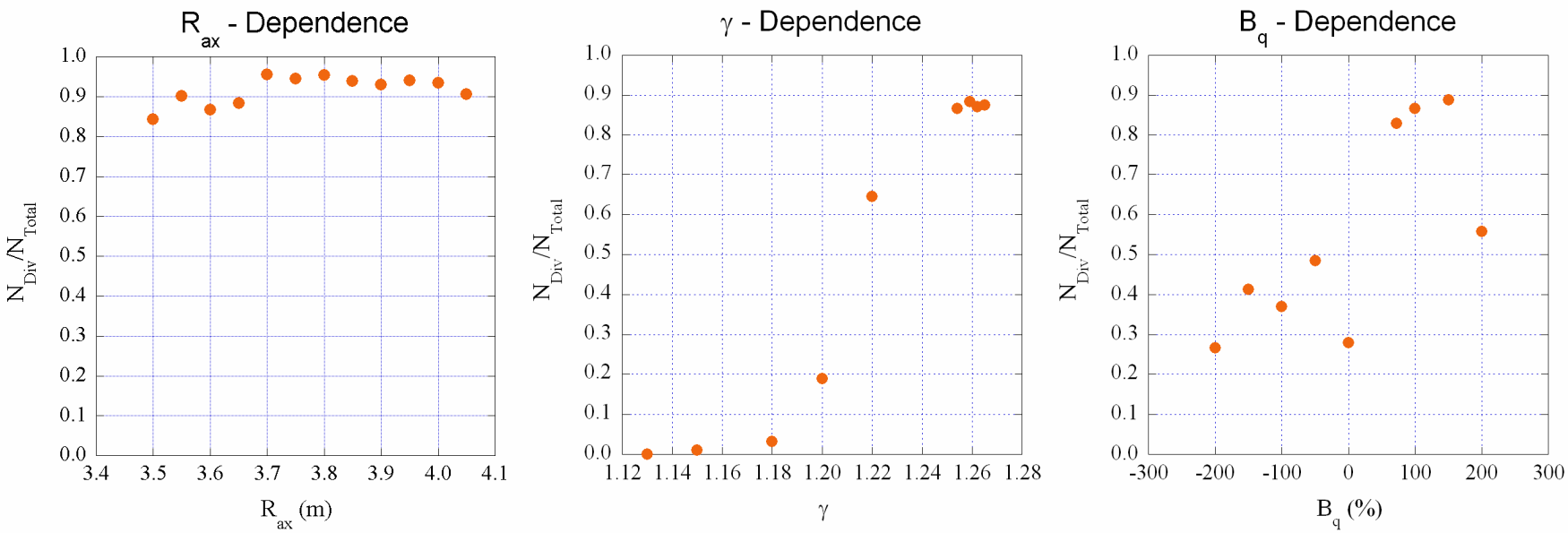

More than 80% of the strike points locate on the divertor plates for all magnetic axes (3.50m<R_{ax}<4.05m). The strike points significantly deviate from the divertor plates for low γ (γ<1.22). The B_q dependence shows that the ratios is less than 60% except for around B_q=100%.

→ Installation of additional divertor plates or restriction of operational range

Observation of Bright Lines and Flakes in a Low γ Case

R_{ax}=3.60m, γ=1.174, B_q=100%, B_{ax}=1.5T

t=1.10s

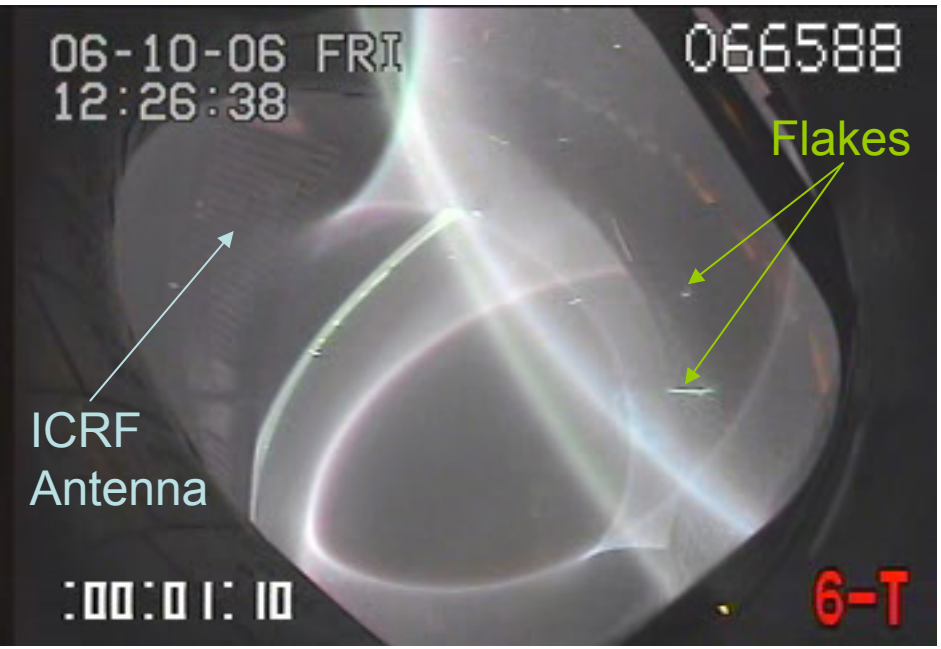

t=1.20s

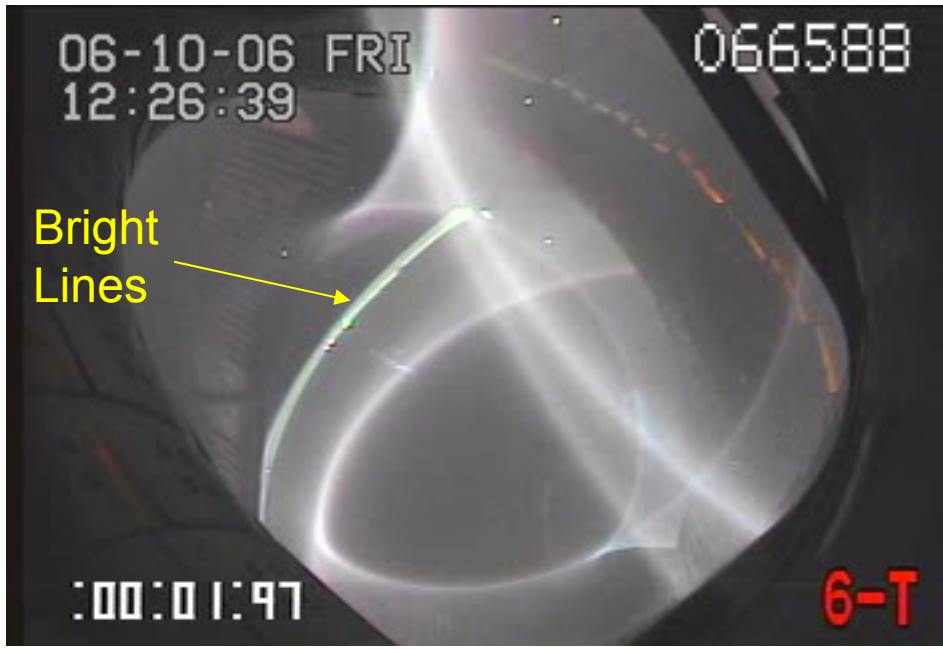

We recognized that the bright lines near an ICRF antenna observed from a tangential port (6-T) in low γ cases originate from the plasma-wall interaction at the side wall of a helical coil can. High heating power operations or long pulse discharges should be minimized to protect the vacuum vessel in LHD.

Summary

Complicated structures of the visible emission profile have been observed with tangentially viewing CCD cameras, which strongly depend on the magnetic parameters (γ, R_{ax}, B_q).

- γ-Dependence
  Expansion of the area of the visible emission profile in the minor radius
- R_{ax}-Dependence
  Transition of the bright area on the divertor legs
- B_q-Dependence
  Deformation of the profile of the visible emission

These dependences are explained by the change of the magnetic field line structure in the plasma periphery.

→ Plasma flow along the magnetic field lines is dominant.

Toroidal and poloidal distributions of the strike points in various magnetic configurations are calculated by tracing magnetic field lines with including the three-dimensional geometry of the vacuum vessel, helical coil can and divertor plates.

→ High heating power or long pulse discharge experiments for γ<1.22 and B_q<50% or >150% should be minimized for safe operations in LHD.